RODRIGO MOGOLLÓN ABURTO
Laboratório de Dinâmica e Modelagem Oceânica (DinaMO)

Estudo da Dinâmica Física e Biogeoquímica no Sistema Norte da Corrente de Humboldt (SNCH)

Rio Grande
2015

RODRIGO MOGOLLÓN ABURTO
Laboratório de Dinâmica e Modelagem Oceânica (DinaMO)

Estudo da Dinâmica Física e Biogeoquímica no Sistema Norte da Corrente de Humboldt (SNCH)

Dissertação apresentada ao Instituto de Oceanografía da Universidade de Rio Grande (FURG), para a obtenção de Título de Mestre em Oceanografía Física, Química e Geológica.

Orientador: Paulo Henrique Rezende Calil

Rio Grande
2015

Rodrigo Mogollón Aburto
Estudo da Dinâmica Física e Biogeoquímica no Sistema Norte da Corrente de Humboldt (SNCH)
106 páginas
Dissertação (Mestrado) - Instituto de Oceanografía da Universidade de Rio Grande (FURG).

1. ENSO
2. EL Niño
3. La Niña
4. Humboldt
5. ROMS
6. BioEBUS

Instituto de Oceanografía da Universidade de Rio Grande (FURG)

Comissão Julgadora:

Prof. Dr.
Antonio F. H. Fetter Filho

Prof. Dr.
José H. Muelbert

Prof. Dr.
Paulo H. R. Calil

Dedico esta tesis a mis padres, Juan Carlos y Elena,
quienes con su apoyo y cariño lo hicieron posible.

Epigraph

Si piensas que estás vencido, lo estás.
Si piensas que no te atreves, no lo harás.
Si piensas que te gustaría ganar pero no puedes, no lo lograrás.
Si piensas que perderás, ya has perdido.
Porque en el mundo encontrarás
que el éxito comienza con la VOLUNTAD del hombre.

Todo está en el estado mental.
Porque muchas carreras se han perdido
antes de haberse corrido,
y muchos cobardes han fracasado
antes de haber empezado su trabajo.

Piensa en grande y tus hechos crecerán.
Piensa en pequeño y quedarás atrás.
Piensa que puedes y podrás.

Todo está en el estado mental.
Si piensas que estás aventajado, lo estás.
Tienes que pensar duro para elevarte.
Tienes que estar seguro de ti mismo
antes de intentar ganar un premio.

La batalla de la vida no siempre la gana
el hombre más fuerte, o el más ligero,
porque, tarde o temprano, el hombre que gana
es el que cree poder hacerlo

Dr.Christian Barnard

Acknowledgements

Agradezco al programa de Oceanografía de la FURG y a la OEA, quienes me brindaron apoyo en todo momento desde el día que llegué a Brasil; a mi orientador Paulo Calil, por su tolerancia e instrucción, a todos mis colegas de laboratorio (never abandons!), a mi familia y amigos, quienes siempre me han apoyado en cada decisión que he tomado en mi vida, y a todas las personas que de alguna manera me incentivaron a seguir adelante a lo largo de estos dos años.

Infinitamente agradecido, profesor Jorge Quispe, por haberme inicializado en mi formación y gracias a usted haber conocido excelentes personas quienes como el Dr. Andrés Sepúlveda y el Dr. Patrick Luyten, me encaminaron a una formación científica de calidad por el futuro de las ciencias del mar en nuestro país.
Gracias Osmar Moller por su invitación al crucero SAMOC X, y a todos mis colegas de Argentina por tan enriquecedora experiencia.

Que esta tesis sirva de ejemplo del sacrificio, esfuerzo y superación que tenemos que ponerle a nuestros objetivos en la vida, y sé que tú mañana recorrerás también mi camino; ánimo.

Finalmente agradezco a Dios de haberme dado la dicha de pasar unos momentos inolvidables junto a mi familia en Cassino, a mis 3 mejores amigos, Héctor, Ricardo y al amigo Parce, por su grata visita...y a ti, a quien siempre recordaré con cariño y agradecimiento, por tu tiempo, comprensión y apoyo; y que de alguna manera, este trabajo lleva también un pedazo de ti.

Gracias

Resumo

O impacto na produção primária e a resposta da biogeoquímica, modulada pelos eventos do ENOS (El Niño Oscilação do Sul) no Sistema Norte da Corrente de Humboldt (SNCH) é avaliada por meio de um modelo acoplado (físico−biogeoquímico) que resolve a mesoescala. Os eventos El Niño (EN) 1997-1998 e La Niña (LN) 1999-2000 são reproduzidos, conduzindo significativas mudanças na distribuição espacial, temporal e na intensidade das variáveis físicas, dos traçadores biogeoquímicos, assim como na estrutura da circulação em 5 importantes centros de ressurgência costeira ao longo da costa peruana (Punta Falsa 6°S, Chimbote 9.4°S, Callao 12.1°S, Pisco 14°S, San Juan 15.7°S). Estas simulações foram forçadas com ventos realistas do NCEP-CFSR e com forçantes laterais a partir do SODA . A produção primária parece ser limitada pela falta de nutrientes durante a fase EN em todos os locais, entretanto durante LN, a Energia Cinética Turbulenta (ECT), devido à intensificação dos ventos Alísios, desempenha um papel chave na perda de nutrientes do inventário costeiro, advectando nitrogênio desde a região costeira para o oceano oligotrófico sul, levando a uma redução da produção biológica. Quantificamos a contribuição do Anammox e da denitrificação na remoção do nitrogênio, os mecanismos envolvidos no suprimento das máximas concentrações de nitritos, e a emissão do óxido nitroso, durante eventos ENSO; encontramos que todos estes processos são modulados pelas condições das concentrações de oxigênio do ambiente, devido à variabilidade espaço−temporal da Zona Mínima de Oxigênio (ZMO) através de El Niño (fase de ventilação) e a oposta fase La Niña. Adicionalmente, foi testada a hipóteses da deflecção na linha de costa em Piso−Paracas e a sua influência em controlar a intrusão das massas de água anômalas durante picos El Niño.

Palavras-chave: ENOS, El Niño, La Niña, Humboldt, ROMS, BioEBUS,

Abstract

The impact on primary production and the response of the biogeochemistry, modulated by extreme events as ENSO in the Northern Humboldt Current System, is assessed by an eddy-resolving numerical simulation using a coupled physical-biogeochemical model. El Niño (EN) 1997-1998 and La Niña (LN) 1999-2000 are well reproduced, leading to dramatic changes on the spatial distribution, intensity and timing of the physical variables, as biogeochemical tracers and the circulation structure at five different important upwelling coastal centers along peruvian coast (Punta Falsa 6°S, Chimbote 9.4°S, Callao 12.1°S, Pisco 14°S, San Juan 15.7°S). These simulations were forced with realistic NCEP-CFSR winds and with SODA lateral forcings. The primary production appears to be limited by nutrients during EN phase at all locations, whereas during LN phase, Eddy Kinetic Energy (EKE), due to intensification of the Trade winds, plays a key role of leaking coastal nutrients inventory, advecting nitrogen from the nearshore region to oligotrophic ocean in the southern locations, leading to a reduction of biological production related with the northern upwelling centers. We quantified the contribution of anaerobic ammonium oxidation (anammox) and denitrification on the removal of nitrogen, the mechanisms involved in the supplying of maximum nitrite concentrations, and the outgassing of nitrous oxide during ENSO events. we found that all of these processes are modulated by the oxygen conditions in the environment due to the spatiotemporal variability of the Oxygen Minimum Zone (OMZ) through El Niño (ventilation phase) and the opposite La Niña phase. An additional hypothesis was tested in order to evaluate the impact of the bend of the coastline at Pisco−Paracas in controlling the intrusion of anomalous water masses during El Niño peaks.

Keywords: ENSO, El Niño, La Niña, Humboldt, ROMS, BioEBUS,

Acronyms

Anammox	Anaerobic ammonium oxidation
AOU	Apparent Oxygen Utilization
AVHRR	Advance Very High Resolution Radiometer
CARS	CSIRO Atlas of Regional Seas
CC	Climatological Conditions
CFSR	Climate Forecast System Reanalisys
Chla	Chlorophyll-a
COADS	Comprehensive Ocean-Atmosphere Data Set
CTW	Coastal Trapped Waves
DON	Dissolved Organic Nitrogen
EBUS	Eastern Boundary Upwelling System
ECCO	Estimating the Circulation and Climate of the Ocean
ECCOsim	ROMS climatological simulation using ECCO boundary conditions

ECS	Equatorial Current System
EKE	Eddy Kinetic Energy
EN	El Niño
ENSO	El Niño Southern Oscillation
EOF	Empirical Orthogonal Function
ESO	Equatorial Sourthern Oscillation
ETOPO2	2-minute Gridded Global Relief Data
ETP	Eastern Tropical Pacific
EUC	Equatorial Undercurrent
hadv	Horizontal advection
hmix	Horizontal mixing
IEKW	Intraseasonal Equatorial Kelvin Waves
IMARPE	Instituto del Mar de Peru
KE	Kinetic Energy
LN	La Niña
LPHYTO	Large phytoplankton
MODIS	Moderate-resolution Imaging Spectro radiometer
N_2O	Nitrous oxide gas
NCEP	National Center for Environmental Prediction
NH_4	Ammonium

NHCS	Northern Humboldt Current System
NO_2	Nitrite
NO_3	Nitrato
NOAA	National Oceanic and Atmospheric Administration
NPP	Net Primary production
OGCM	Ocean General Circulation Model
OMZ	Oxygen Minium Zone
ONI	Oceanic Niño Index
PAR	Photosynthetically Active Radiation
PCC	Peru Coastal Current
PCCC	Peru-Chile Countercurrent
PCS	Pery Chile System
PCUC	Peru Chile Undercurrent
PNM	Primary Nitrite Maximum
PP	Primary Production
pSSCC	primary Southern Subsurface Countercurrent, primary Tsuchiya jet
QuickSCAT	NASA's Quick scatterometer
RClim	ROMS-BioEBUS climatological simulation
RnoPar	ROMS simulation of 1997 with modifications at the coastline
ROMS	Regional Oceanic Modeling System

SeaWIFS	Sea-Viewing Wide Field-of-View Sensor
SEC	South Equatorial Current
SMS	Source minus Sink
SNM	Secondary Nitrite Maximum
SODA	Simple Ocean Data Assimilation
SODAsim	ROMS climatological simulation using SODA boundary conditions
SOI	Southern Oscillation Index
SPHYTO	Small phytoplankton
SSS	Sea Surface Salinity
sSSCC	secondary Southern Subsurface Countercurrent, secondary Tsuchiya jet
SST	Sea Surface Temperature
vadv	vertical advection
VGPM	Vertically Generalized Production Model
WOA	World Ocean Atlas

List of Figures

List of Tables

Contents

Chapter 1

Theoretical Background

1.1 ENSO: Neutral, warm and cool phase

The oceans cover about 70 % of the surface of the Earth. The Pacific Ocean is the largest contiguous body of water, having a tremendous impact on how heat is absorved and redistributed by the ocean as a whole. Under normal conditions, Trade winds blow across the surface of the Tropical Pacific from the southeast (northeast) to the northwest (southwest) in the Southern hemisphere (Northern hemisphere), driving oceanic currents carrying waters from the east to the west and recirculating around the Pacific basin closing a loop and forming the South and North Subtropical Pacific Gyre.

Trade winds pile up warm waters westward, rising the western Pacific sea level (about 0.5m), bringing also cool waters from subsurface at the Eastern Pacific by coastal upwelling, resulting in 8°C to 10 °C sea surface temperature difference between both sides of the Pacific basin. The warm pool at Western Pacific releases heat through evaporation as the moist and warm air rises. As it continues rising, the cooler air reaches the saturation point, releasing it as rain, and the drier remaining air now sinks in the Eastern Pacific meanwhile Trade winds are always replacing the rising air at the

western boundary; this circulation is known as the Walker Cell. As the Trade winds are always supplying energy for piling warm waters at western Pacific, a balance between wind forcing and gravity is established, maintaining this sea level gradient along the Pacific basin as a normal (but not stable) condition.

The temperature difference between the western and the eastern Pacific reinforce the Trade winds, because the western warm pool that heats the air above it (rising air mass) creates a low preassure (LP) zone and the cold tongue water mass at the Eastern Pacific (where the dry air sinks) creates a high pressure zone (HP), and this longitudinal difference of air preassure at the extrems of the Pacific basin enhance the wind to blow, revealing a strong coupled interaction ocean-atmosphere with a positive feedback loop called the Bjerknes feedback, in other words the Trade winds maintain the temperature gradient (and air preassure difference) between Eastern and Western Pacific and this temperature difference keeps Trade winds blowing.

Weather events and also turbulence at the sea-air interface sometimes leads to a generation of eastward fluxes counteracting the westward Trade winds, but usually it get recover again. Every 4 to 7 years a weakening of the Trade winds occurs in which it can not recover. This leads to the generation of a perturbation that propagates eastward carrying anomalously warm waters to Eastern Pacific, as Equatorial Kelvin wave. While these waves travel along the equator it sink the thermocline overcoming any remaining oceanic 'normal condition'. In general, gravity acts to restore the piled water at the west carrying it eastward and flattening the sea level gradient along the basin. It takes about 2 months to reach the west coast of South America travelling at velocities about 200 Km per day and that is when El Niño (EN) begins. Once EN is established, warm water sloshes east, covering a greater surface area resulting in more evaporation and in a displacement of the Walker Cell to the east, leading to the gener-

ation of temporal westerlies at the west Pacific that start to blow in a reverse direction related with the original trade winds direction, in order to feed the rise of spread warm and moisty air mass across the tropical Pacific. A transgression of equatorial water masses at the Peruvian coast are seen when strong EN are settle down like 1997-98 extremely warm phase which rised the SST more than +5°C. Sometimes the warm water does not need to travel until the coast of the America to be declared as El Niño phase, because central Pacific El Niño event could also be possible, what is called El Niño Modoki; which is a weaker EN phase than the classic EN which extends all along to the east.

On the other hand, during LN phase, the Trade winds are stronger and push warm water farther west, allowing further extention of the cold tongue in the east Pacific; basically , LN is an exaggerated ENSO-neutral phase related with an increment of primary production in the NHCS due to enhanced wind-driven upwelling. Because the Trade winds now are blowing more intensely, there is a lack of cloud cover, more visible sunlight (downward shortwave radiation) reaches the surface of the tropical Pacific; this radiation penetrates more than 100 m decreasing in strength with depth. The aditional sunlight warms the tropical Pacific more than normal, increasing the heat content of the ocean. Ocassionaly, a LN event supplies more heat than was discharged by this previous EN, leading to an extremely subsequent EN event. However EN and LN events are not always intercalated, so we should proceed with caution when refering to ENSO events as a periodical phenomenum.

1.1.1 ENSO Index

The traditional indicator of the ENSO state is the Southern Oscillation Index (SOI), which measures the difference between the atmospheric pressure at sea level at Tahiti (18°S) and at Darwin (12°S). When the preassure becomes below average in Tahiti and above average in Darwin, the SOI becomes negative, indicating El Niño phase. In the opposite case, the SOI becomes positive, indicating La Niña. The limitation of the SOI index is the fact that Darwin and Tahiti are located somewhat south of the equator.

The Equatorial Southern Oscillation Index (ESOI), uses the average sea level pressure over two large regions centered at the equator (5°S to 5°N) over Indonesia and the eastern equatorial Pacific, however, data for this index only extend back to 1949, in contrast to SOI which goes back to the late 1800s.

Sea surface temperature data is increasingly used because the ocean was recognized to be a key player in ENSO impact. Initially, certain regions were defined for measurements, namely Niño1, Niño2 (combined into Niño1+2), Niño3 and Niño4, because of consistently available data coming from ships passing through those areas (see Figure 1.1). Later, an area called Niño3.4 was identified as being the most ENSO-representative located between (and overlapping with) Niño3 and Niño4, this is the region whose temperature anomaly is reflected in the ONI, the Oceanic Niño Index, the official ENSO indicator, which is based on SST in the eastern tropical Pacific.

Figure 1.2 summarized these 3 indexes. We used the official ONI index for temporal and intensity ENSO reference.

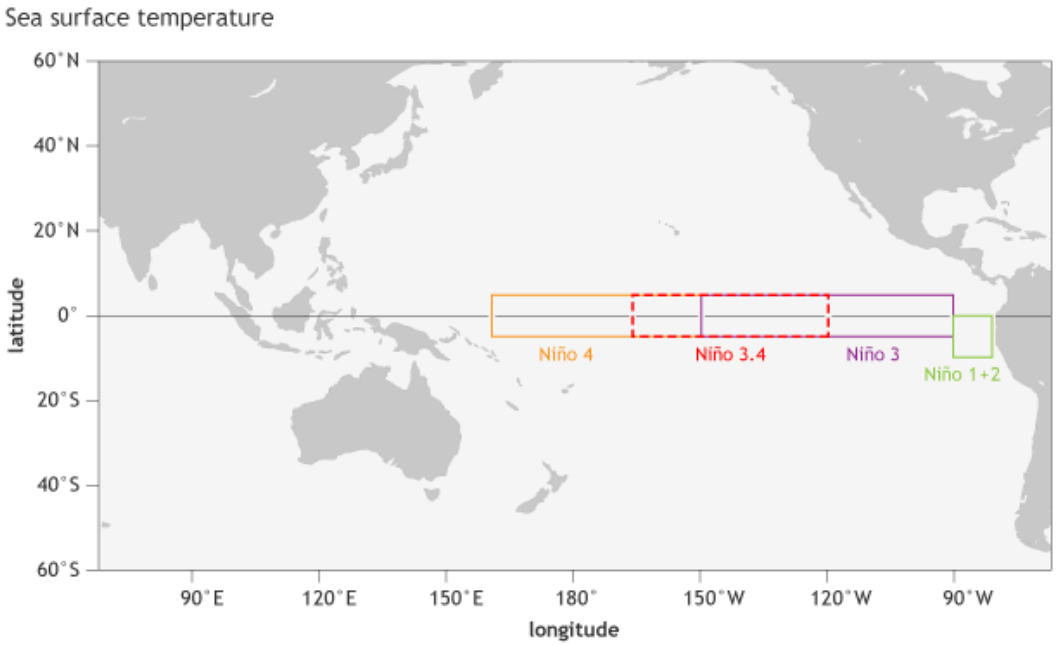

Figure 1.1: El Niño Regions

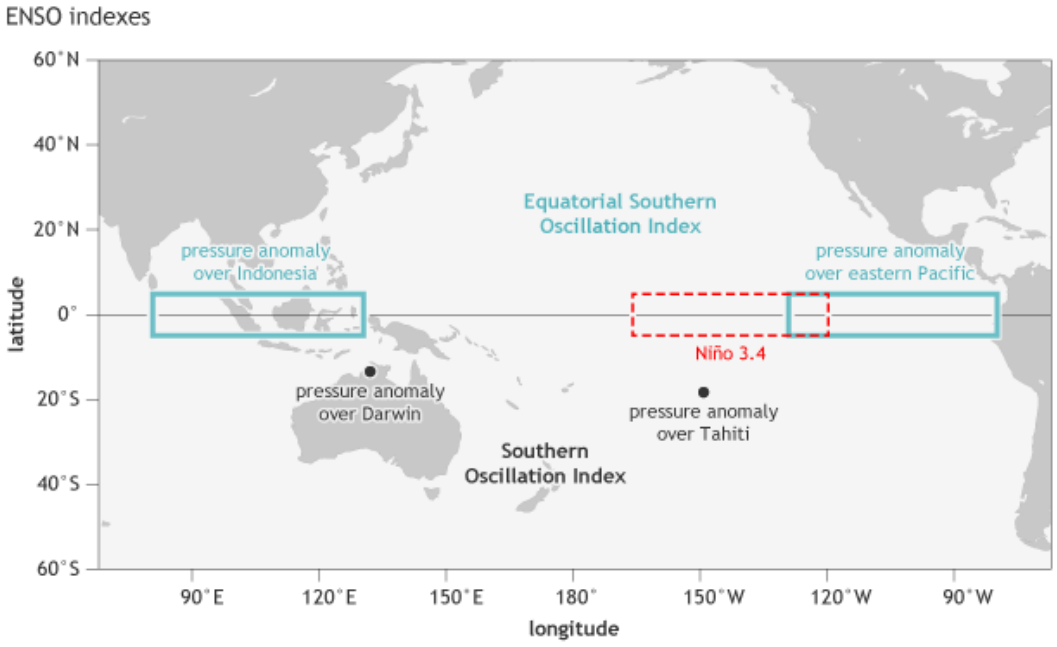

Figure 1.2: ENSO Indexes: SOI, ESOI and ONI.

1.2 Nitrogen Cycle

The majority of the atmosphere of the Earth is composed by nitrogen (78%) and at the same time is the most common limiting nutrient in the ocean. Nitrogen is necessary for all known forms of life on Earth and in the marine ecosystem it only could be assimilated in different reactive forms, like ammonium (NH_4) or nitrate (NO_3); there is also a special case for this uptaking preference, the cyanobacterias, who can fix nitrogen directly from the atmosphere. In general, animals release nitrogen by excretion of NH_3 (terrestrial) or urea $(NH_2)_2CO$ (aquatic), because they can not oxidize ammonium, and these production of ammonium is called ammonification. The avaliability of nitrogen in a system can affect the rates of biogeochemical processes, including primary production, so it is important to understand their spatiotemporal variability in one of the most productive regions in the world (NHCS) and how it is affected by ENSO events. The most important processes related with the bacterial loop are summarized below.

1.2.1 Nitrification

Nitrification is the biological oxidation of ammonium to nitrate, performed by aerobic organisms (using oxygen as electron receptor) in order to obtain energy and consist in two different steps.

$$\xrightarrow{Oxidation}$$
$$NH_4 \xrightarrow{N1} NO_2 \xrightarrow{N2} NO_3$$

Ammonium oxidation

The first step of nitrification (N1) is called Ammonium oxidation, which is the oxidation of the ammonium to nitrite in the presence of the oxygen performed by bacterias as Nitrosomonas and Nitrosococcus. $NH_4^+ + O_2 \rightarrow H^+ + H_2O + NO_2^- + \text{Energy}$

Nitrite oxidation

The second step of nitrification (N2) is the oxidation of the nitrite to nitrate in the presence of the oxygen performed by Nitrobacterias. $NO_2^- + O_2 \rightarrow NO_3^- +$ Energy

1.2.2 Denitrification

A stepwise reduction process involving a number of intermediates (gaseous products of oxides of nitrogen) which produce molecular nitrogen (if it has been completed). The first step of denitrification (D1) is the reduction of the nitrate to nitrite in the absence of the oxygen performed by heterotrophic bacterias, as Pseudomonas fluorescens in order to obtain energy. The denitrification is a fundamental process which return nitrogen to the atmosphere and is often called as the opposite process of fixation. (nitrogen uptaking from the atmosphere).

$$\xrightarrow{Reduction}$$

$$NO_3 \xrightarrow{D1} NO_2 \rightarrow NO \rightarrow N_2O \uparrow \rightarrow N_2 \uparrow$$

$$\text{nitrate} \rightarrow \text{nitrite} \rightarrow \text{nitric oxide} \rightarrow \text{nitrous oxide gas} \rightarrow \text{nitrogen gas}$$

There is also another important process called Dissimilatory nitrate reduction to ammonium (DNRA) which is considered as the opposite process to the nitrification. Is the conversion of nitrate and nitrite (reduction process) to ammonium (also releasing nitrous oxide gas) performed by Citrobacters under fully anoxic environments.

1.3 General objective

- Assess how physical and biogeochemical processes are affected by large scale changes in the physical environment in coastal areas in the Northern Humboldt Current System (NHCS) at extreme ENSO events.

1.4 Specific objectives

- Modelling the Peruvian Current System (PCS) with their Equatorial connections.
- Reproduce extreme ENSO events: El Niño 1997-98 and La Niña 1999-2000.
- Assess the main important latitudinal changes in the coastal circulation and nearshore processes.
- Analyze and quantify the spatial-temporal variability of nutrients and oxygen contents, as well as the main oxygen-dependent processes.
- Suggest some biogeochemical indicators for monitoring ENSO events.

Chapter 2

Manuscript

2.1 Introduction

The Humboldt Eastern Boundary Upwelling System (EBUS) is considered one of the most productive systems. Located at the Eastern Tropical Pacific (ETP) along the coast of Peru and Chile (Pocklington, 1981), it is responsible for more than 20% of the worldwide marine fish catch; important fisheries such the 'anchoveta peruana' (*Engraulis ringens*), are one of the mainstay of the economy of Peru (Zuta and Guillén, 1970). The Humboldt System is very sensitive to equatorial oceanic perturbations because of the proximity and direct connections with the Equatorial Current System (ECS) (Montes et al., 2010) and, for being at low latitudes, strong divergence Ekman transport is allowed due small Coriolis parameter, feeding this intense permanent coastal upwelling.

High biological activity along the Peruvian coast results from yearlong coastal upwelling due to the Trade Winds (Strub et al., 1998), which maintain a horizontal pressure gradient along the coast associated with a coastal geostrophic current flowing towards the Equator (The Humboldt Current), inducing vertical advection of cold and nutrient rich waters from the subsurface. This upwelling−favorable wind is intensified

in austral winter, sustaining high levels of biological productivity, inducing high rates of aerobic remineralization (consumption of oxygen by descomposition of the organic matter), permiting the development and the maintenance of one of the major Oxygen Minimum Zone (OMZ) (Paulmier and Ruiz-Pino, 2009) (Fuenzalida et al., 2009) , which in the last 50 years, has been expanding (horizontally and vertically) and intensified (Stramma et al., 2008), affecting the biodiversity and distribution (Stramma et al., 2010).

The coastal nutrient inventory that is normally supplied by coastal upwelling from relatively shallow depths (50m -100m) (Zuta and Guillén, 1970) (Pocklington, 1981), is affected in terms of vertical flux of advected nutrients to the upper layer of the ocean which is afterward becomes advected offshoreward , during large scale forcings and remote variability, as the Interannual Equatorial Kelvin Waves (IEKW) which are generated during the ENSO events. When these IEKW arrived to the coast of South America, they propagate southward as Coastal Trapped Waves (CTW) (Belmadani et al., 2012), producing a vertical displacement of the pycnocline and nutricline (Echevin et al., 2014), modulating the inflow and outflow of nutrients above the euphotic layer (Colas et al., 2008) The amplitudes of the IEKW and also the subsequent triggered CTW, are modulated at interannual time scales like (Lengaigne, 2002); as it happened during 1997-1998 El Niño, when the nutricline sank along the coast of South America, leading to a drastic change of all trophics levels (Carr, 2002),(Ulloa et al., 2001) , therefore ENSO events (El Niño and La Niña) will have a dramatic impact on distribution of nutrients and primary production as well.

Important biogeochemical processes such as denitrification and Anaerobic ammonium oxidation (Anammox) , associated with the microbial loop, take place within the OMZ (concentrations lower than 0.5 ml O_2 l^{-1} or 25 mmol O_2 m^{-3}). These processes lead to a loss increase of fixed oceanic nitrogen from the ocean, emitting nitrous oxide (N_2O) to the atmosphere, which is a well known greenhouse gas with a warming potential 300 times more efficient than CO_2. The global ocean contributes with 40% from the global emissions of N_2O (Bange, 2006), meanwhile almost a half of these oceanic contribution is attributed to coastal upwellings as the main source regions (Nevison et al., 2003).

Great efforts have been done to understand the changes on the physical dynamics in the NHCS through ENSO events (Colas et al., 2008) (Montes et al., 2011) (Echevin et al., 2014)), however it is important to predict how the biological productivity will react in the face of climatic changes and how does the physics controls the biogeochemical processes which have a huge socio-economic impact in countries as Peru. This will be particulary true during perturbation events such as ENSO. Hence we have designed numerical experiments that simulates this interannual variability from 1995 to 2000; this period was specially selected for presenting extreme ENSO events in the warm phase, such as El Niño 1997-1998, and also in the cold phase, La Niña 1999-2000.

2.2 Methodology

2.2.1 Hydrodynamic Model

In this study, the employed model is the Regional Oceanic Modeling System (ROMS-AGRIF). The reader is referred to Shchepetkin and McWilliams (2005) and Shchepetkin and McWilliams (2009) for a more complete description of the physical model. ROMS is a split-explicit, free surface oceanic model that solves the primitive equations, based on the Boussinesq approximation and hydrostatic vertical momentum balance. ROMS is vertically discretized in sigma coordinates or terrain-following curvilinear coordinates. It contains also a package of Matlab scripts called Romstools (Penven et al., 2008) that improve the creation of the pre-processing files.

2.2.2 Biogeochemical Model

The nitrogen-based biogeochemical model especially developed for EBUS, called BioEBUS (Gutknecht et al., 2013a), is derived from $NPZD-$like model Koné et al. (2005), with an explicit equation for oxygen with the source term (photosynthesis) and sink terms (zooplankton respiration, bacteria remineralization) as well as the sea-air O_2 fluxes. It also includes O_2-dependent processes, such ammonification/nitrification (under oxic conditions) and denitrification/anammox (under suboxic conditions). The model contains 12 compartments; phytoplankton, zooplankton and detritus compartments are split into 2 variables based on a size criterion (small and large), representing the main planktonic communitites: small phytoplankton as flagellates and large phytoplankton as diatoms; while small zooplankton represents ciliates and the larger one, copepods. Compartments of NO_3, NO_2 and NH_4 as inorganic nutrients (nitrate, nitrite and ammonium respectively) and Dissolved Organic Nitrogen (DON) allow us to have a detailed description of the microbial loop. A nitrous oxide N_2O compartment is also provided Nevison et al. (2003). The evolution of all of these biological tracers

concentration C_i is determined by the advective-diffusive equation, as follows:

$$\frac{\partial C_i}{\partial t} = -\nabla.(uC_i) + K_h\nabla^2 C_i + \frac{\partial}{\partial z}(K_z\frac{\partial C_i}{\partial z}) + SMS(C_i)$$

with SMS terms (source-minus-sink) for each compartment, due to biological activity. Biological model parameters (see table 2.1) are similar to the ones used in Montes et al. (2014) who fit the modeled oxygen and nitrate fields to observations; and the remaining values are kept as in the original version used in previous studies in other EBUS (Benguela). The reader is referred to Gutknecht et al. (2013a) and Gutknecht et al. (2013b) for more detailed information about the model.

2.3 Model Set up

2.3.1 Domain

The domain used in all numerical experiments in this study spans the region between 70°W to 90°W and from 5°N to 20°S (Figure 2.1), encompassing the whole of the Northern Humboldt Current System and the adjacent Eastern Tropical Pacific, which connects the equatorial zonal currents with the Peru-Chile System (PCS). This has to be taken in consideration in order to be able to succesfully reproduce the PCS circulation structure. (Montes et al., 2010), (Echevin et al., 2011).

Table 2.1: Parameters of the biogeochemical model as in Gutknecht et al. (2013a) Gutknecht et al. (2013b) and Montes et al. (2014)

Parameter	Value	units
Seawater light attenuation	0.04	m^{-1}
Chl-a light attenuation	0.024	$m^2(mgChl)^{-1}$
Carbon to Nitrogen ratio	106/16	$molC(molN)^{-1}$
Ratio of O_2 to N	170/16	$molO_2(molN)^{-1}$
Ratio of Chl to C	0.02	$mgChla(mgC)^{-1}$
Half-sat. for oxic descomposition	55	$mmolO_2m^{-3}$
Sinking velocity for Lphyto	0.5	$mday^{-1}$
Small Phytoplankton		
Half-sat. for $NO_3^- + NO_2^-$ uptake	0.5	$mmolNm^{-3}$
Half-sat. for NH_4^+ uptake	0.5	$mmolNm^{-3}$
Max. growth rate at 0°C	0.557	day^{-1}
Large Phytoplankton		
Half-sat. for $NO_3^- + NO_2^-$ uptake	2.0	$mmolNm^{-3}$
Half-sat. for NH_4^+ uptake	1.0	$mmolNm^{-3}$
Max. growth rate at 0°C	0.4	day^{-1}
Nitrification		
Rate of 1st stage	0.09	day^{-1}
Rate of 2st stage	0.25	day^{-1}
Denitrification		
Rate of 1st stage	1.2	day^{-1}
Rate of 2st stage	2.0	day^{-1}
Anammox		
Anammox constant	0.1	day^{-1}
Detritus		
Hydrolysis rate of SDET	0.06	day^{-1}
Hydrolysis rate of LDET	0.04	day^{-1}
SDET sinking velocity	1.0	$mday^{-1}$
LDET sinking velocity	40	$mday^{-1}$

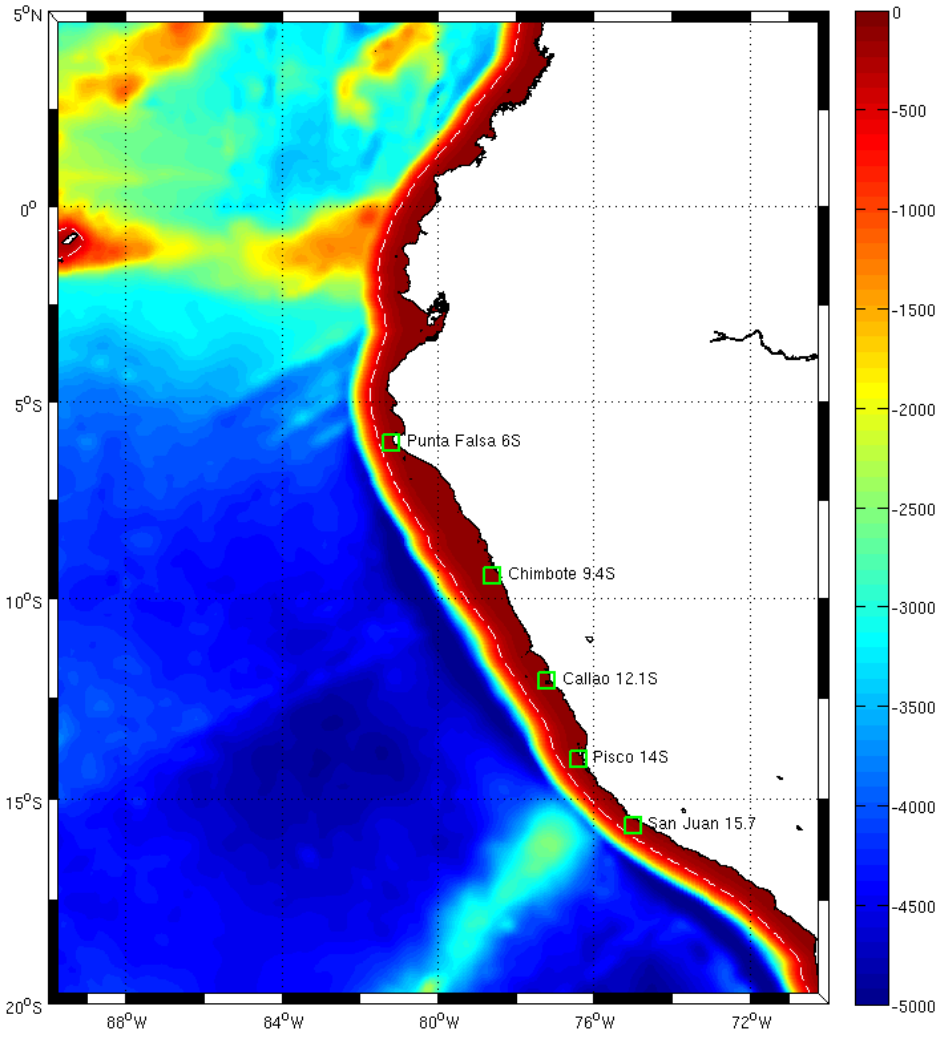

Figure 2.1: Map of model domain. Colors represent the bathymetry [m]. Green squares (2500 km^2) are the upwelling centers chosen for our analysis. White line indicates the 500m depth isobath.

2.3.2 Spatial resolution

Due to computer limitations, we have choosen a horizontal resolution of 1/10 (i.e 11 Km) with 32 vertical sigma levels stretched toward the surface, that allows us to have a good refinement at the first 100 m (approximately 15 levels over the continental slope). Our horizontal isotropic grid contains 262 x 202 grid points. The topography is derived from ETOPO2, a 2° resolution database (Smith and Sandwell, 1997) and was smoothed to reduce pressure gradient computation errors (Marchesiello et al., 2003).

2.3.3 Initial conditions

The first experiment consists in evaluating the evolution of the hydrodynamic and the circulation patterns in the domain using two different boundary conditions from two different climatologies from years 1992 to 2000, one derived from ECCO (http://ecco2.jpl.nasa.gov/) and another one, from SODA (Carton and Giese, 2008). ECCO and SODA are oceanic reanalysys products consisting in gridded state variables of the global ocean generated by combining historical ocean observations with an oceanic general ocean model (OGCM) to reconstruct historical changes in the state of the ocean. Although doing a sensibility study of these datasets is beyond our scope, it is important to analyze, at least qualitatively, which one might simulate adequately the circulation in the NHCS to use the last monthly dynamical state of their respective long-term simulation, in order to use it as initial conditions for the second experiment and also, as a choosen dataset for the third experiment (see section 2.3.4) .

The climatological simulations that are performed with ECCO and SODA (hereinafter called ECCOsim and SODAsim respectively), were run for 10 years (only the physical model), with the same initial conditions for both, provided by initial fields of tracers and velocities related to january of 1992 from SODA. At the surface, the ECCOsim and SODAsim are forced with the same heat and fresh water fluxes from COADS monthly climatology (Da Silva et al., 1994); and the monthly wind stress climatology comes from the QuickSCAT satellite scatterometer (Liu et al., 1998).

2.3.4 Boundary conditions

Two main experiments were conducted to assess how the physical forcings are leading the biological tracers within different scenarios with realistic atmospherical (wind stress, as the major contributor of these interannual variability related to ENSO) and oceanographic forcings (velocities and tracers fields provided by an OGCM related with our first experiment).

First of all, building a climatology of the biogeochemical and physical variables was needed, for reserving as a control simulation and also to contruct a new climatology for biological tracers (hereafter RClim). Rclim was run also for 10 years (ROMS+BioEBUS) with the same lateral forcings used for SODAsim and the initial conditions from the last month of SODAsim (see appendix A). The oxygen and nitrate fields were extracted from the CSIRO Atlas of Regional Seas, CARS 2009 [www.cmar.csiro.au/cars]; and the chlorophyll-a concentrations, from SeaWIFS (McClain, 1998), (O'Reilly et al., 1998). The following biogeochemical tracers , are compute internally, using the methodology explained in Gutknecht et al. (2013a) Gutknecht et al. (2013b). Initial phytoplankton is a function of Chl-a and vertically extrapolated from the surface values using the parameterization of Morel et al. (1989) , for zooplankton, a cross-shore profile following in situ observations, with low concentrations offshore and increasing concentrations

onshore. N_2O is a function of O_2 from the CARS database 2009, using the parameterization of Suntharalingam et al. (2012) and Suntharalingam et al. (2000). For the others biogeochemical tracers, a vertical constant profile is used for detritus, and a exponential one, for nitrite, ammonium and Dissolved Organic Nitrogen (DON).

The third experiment consists in simulating years 1995 thru 2000 (climatologically simulated each year) using the same year to year climatology constructed in RClim for boundary conditions related to biological tracers ; the physical fields were provided by monthly SODA datasets for each year, and we have used the final state of RClim to begin year 1995. The remaining years (1996-2000) begin with the conditions of december of their respective previous year.
At the surface is forced with the same heat and fresh water fluxes from COADS monthly climatology ; and the winds stress fields, extracted from the National Center for Environmental Prediction (NCEP) Climate Forecast System Reanalisys (CFSR) datasets (Saha et al., 2010) monthly averaged for each year. We do not have a realistic interannual variability in our boundary conditions related with biological tracers, however by proceeding so, we might reproduce the physical impact on climatological biogeochemistry, and reproducing the biological response during ENSO events, which is going to depend on how well represented is the physical variability in our experiments (see section 2.4).

Run	Physics		Biology	
	Boundary	Initial	Boundary	Initial
SODAsim	SODA (1992-2000)	SODAM1Y1992	-	-
ECCOsim	ECCO (1992-2000)	SODAM1Y1992	-	-
RClim	SODA (1992-2000) / QuickSCAT / COADS	SODAsim (M12)	CARS2009 / SeaWIFS(chla)	
Y1995	SODA / NCEP 1995	RClim (M12)	RClim	RClim (M12)
Y1996	SODA / NCEP 1996	Y1995 (M12)	RClim	Y1995 (M12)
Y1997	SODA / NCEP 1997	Y1996 (M12)	RClim	Y1996 (M12)
Y1998	SODA / NCEP 1998	Y1997 (M12)	RClim	Y1997 (M12)
Y1999	SODA / NCEP 1999	Y1998 (M12)	RClim	Y1998 (M12)
Y2000	SODA / NCEP 2000	Y1999 (M12)	RClim	Y1999 (M12)

Figure 2.2: Numerical Experiments

2.4 Validation

2.4.1 Physical Aspects

Sea Surface Temperature (SST)

We compared the seasonal mean SST (°C) between ROMS (averaged last 5 years of simulation of RClim), CARS2009 climatology and the Moderate-resolution Imaging Spectro radiometer (MODIS) (http://modis.gsfc.nasa.gov/) from july 2002 to december 2014, to evaluate the model outputs of our experiments (Figure 2.3). In summer, in all products, we can notice the cold upwelled water along the shore, with an equatoward extended tongue that signatures the upwelling front. High temperatures at northern part of the domain and colder ones at southern part of the domain. In Fall, ROMS shows a better agreement with MODIS with regards to the extension and intensity of the westward strong upwelling filament. In winter, the coastal cold upwelled water is

more confined nearshore at the southern region and during spring, the warmer oceanic tongue that begins to approach at the coast, appears to be more diffuse in ROMS than in the two others, but in general, the large scale pattern is very well captured by the model.

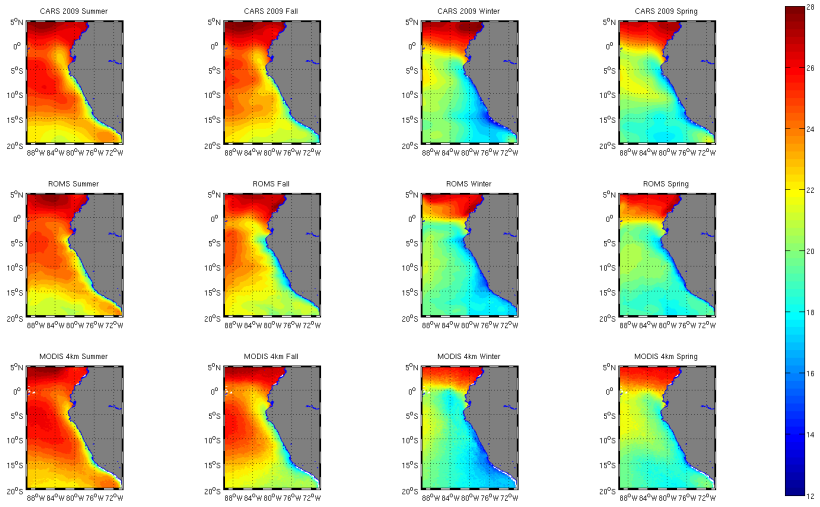

Figure 2.3: Seasonal mean of climatological sea surface temperature comparison between CARS2009 1/2° resolution (monthly averaged since all available historical ocean measurements), ROMS 10 km resolution (annual mean of the last 5 years of RClim) and MODIS 4km resolution (monthly averaged from july 2002 to december 2014). Contour colors are in [°C]

To validate the interannual simulations, we compare the modeled SST with the Advance Very High Resolution Radiometer (AVHRR) Pathfinder (Casey et al., 2010) during 1998 and 1999 for representating the evolution of EL and LN events, (Figure 2.4,2.5). In general, ROMS exhibits a colder bias at the western oceanic domain and also in the middle coastal region during the summer and fall of 1998. ROMS reproduces succesfully the recovery phase of El Niño 1998 (transition since late fall) and the intensification of upwelled colder water that spans over southern domain during La Niña in winter 1999.

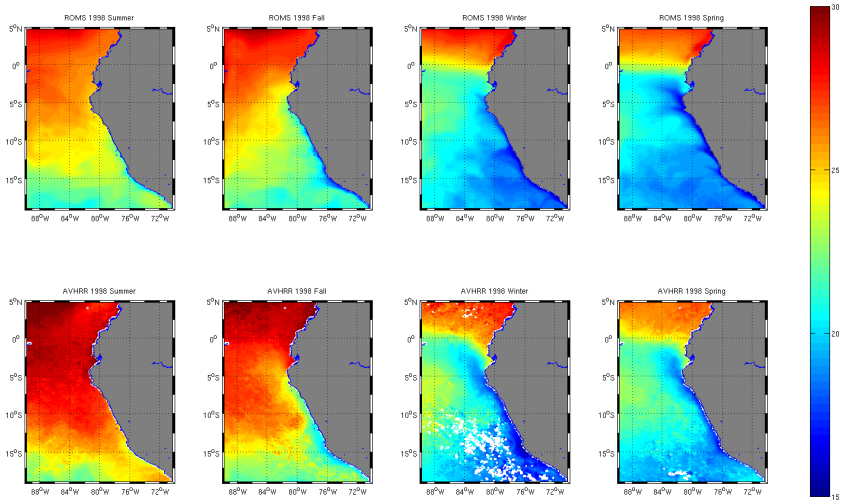

Figure 2.4: Seasonal mean of 1998 sea surface temperature comparison between AVHRR and ROMS. Colors are in [°C]

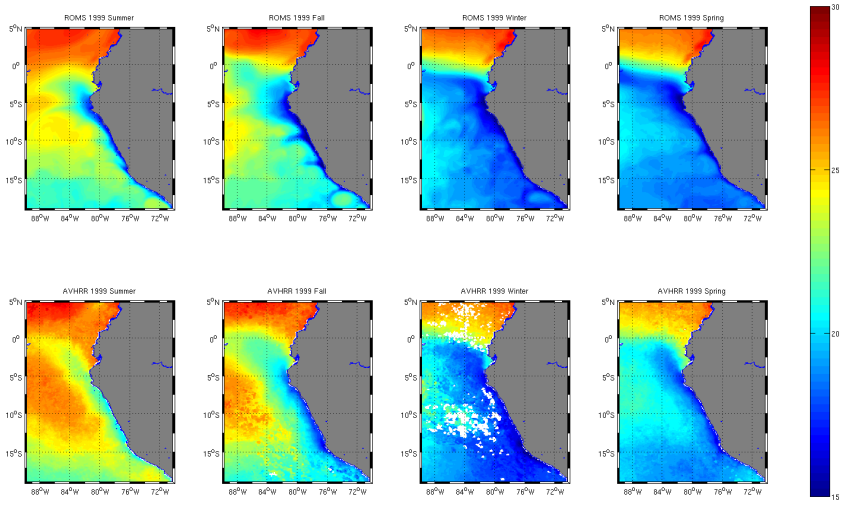

Figure 2.5: Seasonal mean of 1999 sea surface temperature comparison between AVHRR and ROMS. Colors are in [°C]

Sea Surface Salinity (SSS)

Similar maps of SSS were plotted also for comparison, between ROMS, CARS2009 and from the World Ocean Atlas 2013 (Levitus et al., 2013) which salinity climatology is the average of six "decadal" climatologies for the following time periods: $1955-1964, 1965-1974, 1975-1984, 1985-1994, 1995-2004$. The different surface water masses are well reproduce (using the SSS as a proxy) (Zuta and Guillén, 1970) (Strub et al., 1998) (Figure 2.6).

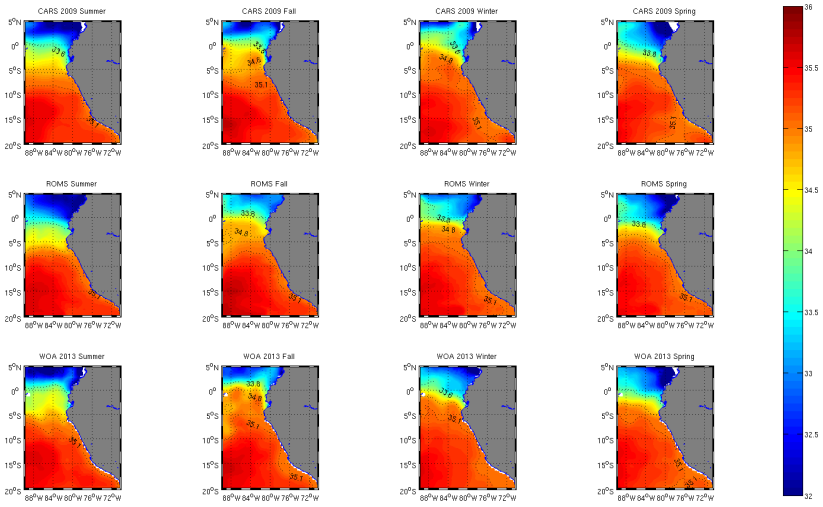

Figure 2.6: Seasonal mean of climatological sea surface salinity comparison between CARS2009 1/2° resolution (monthly averaged since all available historical ocean measurements), ROMS 10 km resolution (annual mean of the last 5 years of RClim) and WOA2013 25km resolution (averaged of 6 decadals means between 1955-2012)

2.4.2 Biogeochemical Aspects

Chlorophyll−a

The simulated annual mean climatological chlorophyll concentration from RClim is compared with SeaWIFS of 9km resolution (averaged from september 1997 to december 2010) and MODIS of 9km resolution (averaged from july 2002 to december 2012) (Figure

2.7); the spatial pattern is well reproduced within the highly productive coastal zone, squeezing southward. It displays a gradual decrease of offshore concentrations, however, coastal concentrations are overestimated northern of Punta Falsa (6°S). The seasonal mean chla concentration of 1998 is also showed for validating our interannual experiment (Figure 2.8); in spite of the cloud coverage, specially in winter, ROMS-BioEBUS appears to being reproducing realistically the spatial distribuition of chla in amplitude and timing. In summer of 1998, a strong decay of surface coastal Chla concentrations is simulated (due to realistic physical EN conditions) and the high concentrations detected in the persistent upwelling filament located northern Punta Falsa, shows that the model exhibits an excessive coastal upwelling, furthermore, the algorithm of SeaWIFS, used to calculate surface Chla from radiance, tends to underestimate high concentrations in coastal zones (Hooker and McClain, 2000), (Echevin et al., 2008).

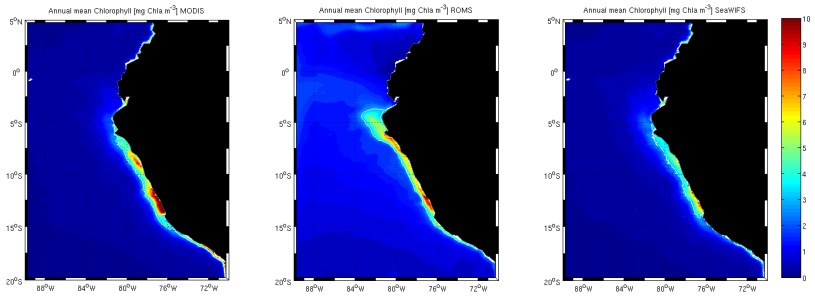

Figure 2.7: Annual mean of climatological chlorophyll concentration in mg chla m^{-3} comparison between SeaWIFS 9km resolution (averaged from september 1997 to december 2010), ROMS (annual mean of the last 5 years of RClim) and MODIS 9km resolution (averaged from july 2002 to december 2012)

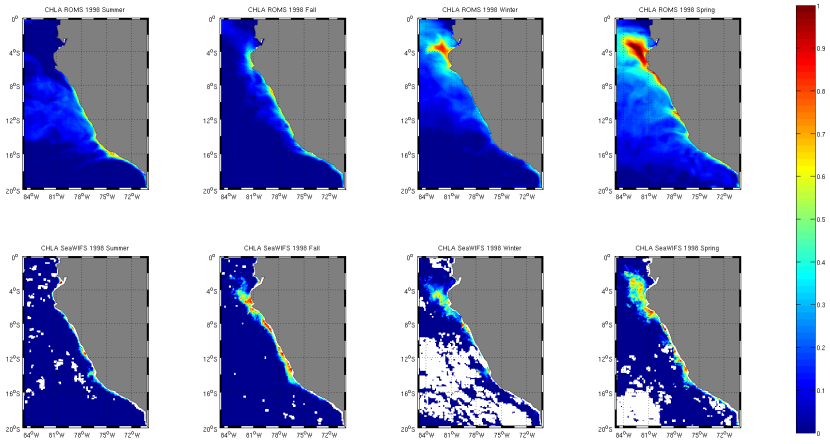

Figure 2.8: Seasonal mean of 1998 chlorophyll concentration [mg log (chla) m^{-3}] comparison with SeaWIFS satellite. Values close to one implies 10 mg m^{-3}

Net Primary Production (NPP)

The 'available' carbon (or their equivalent in nitrogen by Redfield relation) for consumption by the heterotrophic community (after phytoplankton used for their own requirements) is called Net Primary Production. The NPP is a rate of photosynthetic product (organic material created by using sunlight energy and fixation of CO_2 by phytoplankton) that becomes bioavailable after subtracting respiration terms. The Vertically Generalized Production Model (VGPM), a SeaWIFS product for estimating NPP (Behrenfeld and Falkowski, 1997), is a function of Chla, Photosynthetically Active Radiation (PAR) and temperature; the last one uses the AVHRR product. We compare again the years 1998 and 1999 as a seasonal mean, in order to avaliate the modeled NPP. Figure 2.9 and Figure 2.10 show a good agreement between simulated and satellite derived NPP rates, although the coupled ROMS-BioEBUS presented an overestimated bias and appeared to be very sensitive to the variability of limiting growth factors, as temperature, light and nutrient avaliability (see section 2.5.4).

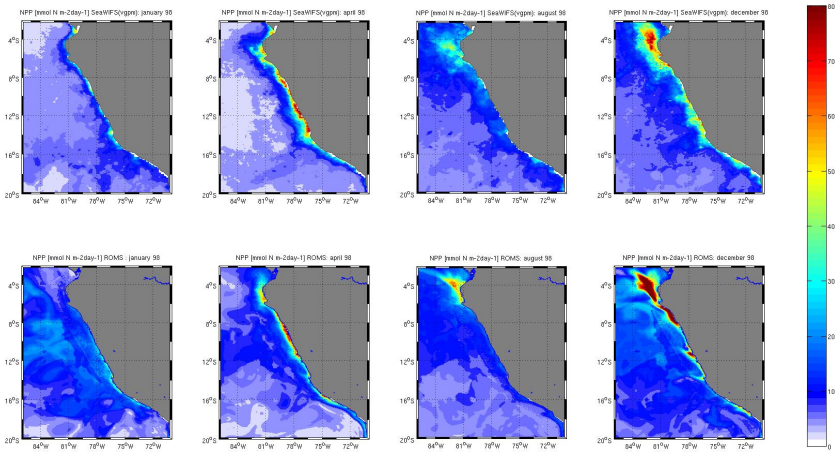

Figure 2.9: Seasonal mean of 1998 NPP rates [mmol N m^{-2} day^{-1}] comparison with SeaWIFS (VGPM method) satellite.

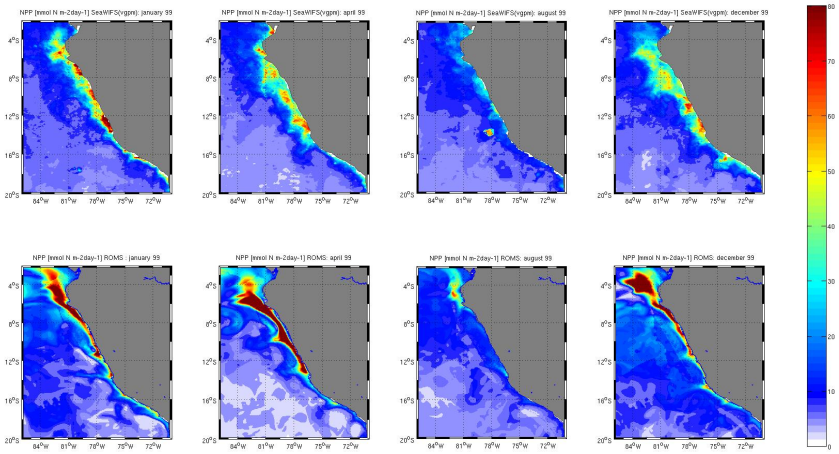

Figure 2.10: Seasonal mean of 1999 NPP rates [mmol N m^{-2} day^{-1}] comparison with SeaWIFS (VGPM method) satellite.

Apparent Oxygen Utilization (AOU)

The AOU, is an indicator of consumed oxygen (respiration, remineralization) which represent the sum of the biological activity in the system. In Figure 2.11, a comparison is presented between WOA2009 1° resolution against RClim. Negative values indicate

regions where production processes, as primary production, leads consumption processes, as respiration.

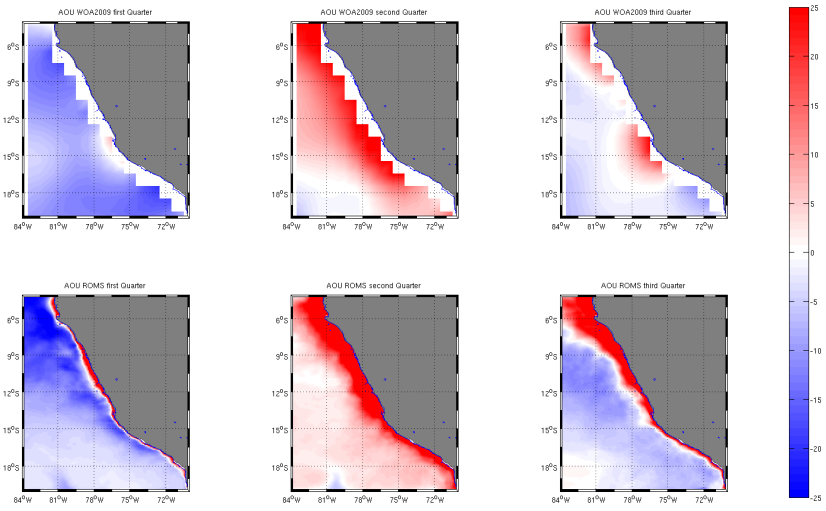

Figure 2.11: 4th-monthly averaged of climatological AOU [mmol O_2 m^{-3}] comparison between WOA2009 database and RClim. Negative values indicates regions where production processes, as primary production, leads consumption processes, as respiration.

In spite of CARS 2009 underestimation of surface nitrate concentrations in our domain (not shown), the coupled model exhibits a rich nutrient region that is closely with realistic values and temporal bias in response of an intense coastal upwelling and mesoscale eddy activity that ROMS performed, leading to better results; after all, these climatological data sets are a numerical guide for not having scattered solutions but at the same time, obtain realistically a well represented pattern. These previous examinations (see Appendix B, C) served to gain reliability in our designed experiments and modeled numerical outputs, given us the confidence in order to proceed with the assumption that biological tracers are also following the same level of reliableness. We now are proceeding to avaliate the biogeochemical response in the next section.

2.5 Results and Discussion

2.5.1 Physical vertical structure

The first section is related with physical changes in the coastal circulation in our 5 locations of study. We summarized the results showing 6 vertical sections of the annual mean state of velocities. Each graph is arranged as follows: the first column displays the cross-shore velocities (positive values implies onshore velocities and negative values offshore velocities), the second one, the alongshore velocities (positive values imply equatoward velocities and negative values poleward velocities); the top images correspond to RClim (Climatological Conditions), the middle images for El Niño conditions (year 1997), and the bottom ones for La Niña conditions (year 1999).

During climatological conditions, a poleward alongshore flow, the Peru-Chile Undercurrent (PCUC), flowing over the continental slope, with a shallower core at 100 m; meanwhile during EN phase, it displays a vertical sink of about 200m with a horizontal spreading, outcropping (from 100 Km offshore) to the surface and acting as a

countercurrent in agreement with Penven (2005). Above the PCUC, a thin and wide Peru Coastal Current (PCC), which during LN conditions becomes faster and wider (more than 15 cm s^{-1}), gets confined in the first 100 Km nearshore during EN phase. The cross-shore velocities display the upwelling scenario, subsurface onshore velocities that feed surface offshore velocities (Ekman transport). As Punta Falsa is the closest location in our study, related to the Equator, is very sensitive to equatorial variability, and the apparent reduction of advection during LN compared with CC conditions is due to the intensification of equatorial subsurface currents Montes et al. (2011) which brings more water into the eastern tropical Pacific. During EN phase, the cross-shore velocities appears to be stronger, maybe associated with the intensifcation of the PCUC, the wind fields (see section 2.5.5) and also a persistent filament in this location which the model tends to overestimate. However the upwelled water are not as nutrient-rich as during CC or LN conditions (see section 2.5.3).

Chimbote, figure 2.13, displays the largest relative changes in relation to other locations; first of all the PCUC is intensified during EN and get weaker and more diffuse during LN, whereas the PCC becomes stronger (equatoward flow due to stronger trade winds). Under climatological conditions, the core of the PCUC flows between 100-200 m depth (6 cm s^{-1}) dominating the continental slope while the PCC flows in the first 50m depth (10 cm s^{-1}). It is noticiable the typycal upwelling pattern developed when focus on the cross-shore velocities. During EN conditions the PCUC outcrops sharply, retaining the PCC over the wider continental shelf (which is probably why it becomes faster). An anomalous water mass enters the domain laterally, which is a signature of the El Niño phase: a surface intensification of the onshore flow which advected stratified, poor-nutrient, oxygen-rich, warmer and lighter waters onto Chimbote, as we can see, a downwelling pattern is now set, advecting nutrient rich water (carried by the PCUC core) offshore while it has been deepening, contributing negatively by exportat-

ing nutrients at greater depths and bringing nutrient-poor waters into the surface; also contribes to ventilate the water column (see section 2.5.3). La Niña periods tends to intensify of climatological conditions, therefore enhancing primary production.

Callao, figure 2.14, because it is located at an intermediate latitude (not enough far or near from ENSO equatorial signal), does not exhibits a relative strong response as the other locations. During CC, the core of the PCUC (6 cm s^{-1}), the coastal equatoward jet (15 cm s^{-1}) and an upwelling pattern are well defined and the changes during ENSO events might be considered as general important changes in the NHCS. During EN the PCUC becomes faster (10 cm s^{-1}), expanding horizontally (250 Km offshore) exhibiting an outcropping at 150 Km offshore. Again, an onshore flow counteracts offshore Ekman transport in the upper layer. and interesting feature is developed between 300m - 650m depth and 50 Km -180 Km distance of the coast, the appearance of an non-identified equatoward current (6 cm s^{-1}) below the PCUC (also seen at Punta Falsa and Chimbote) was also reproduced in Colas et al. (2008) and a similar equatoward current were observed at depth off northern California during El Niño 1997-1998 (Kosro, 2002), it remains unclear the mechanism of this subsurface equatoward current, however it appears to be related with the uplifting of the PCUC during EN phase in response to the incoming greater onshore flux.

During LN phase, a stronger PCC (25 cm s^{-1}) and PCUC (10 cm s^{-1}) is obtained, in agreement with Montes et al. (2011), Colas et al. (2008), correlated with their respective cross-shore velocities. Stronger offshore advection is seen 100 Km off the coast along the water column following the mechanism described in (Gruber et al., 2011), which can be understood by a lateral circulation. Firstly mesoscale induces a horizontal flux in the near-surface ocean within the nearshore 100km associated with mesoscale processes such as filaments. Between 100-300km from shore, the shallow offshore transport by eddies weakens, while a substantial amount of subduction now occurs.

In general, the PCUC at Pisco ,figure 2.16, is deeper and wider extention than other locations. During EN, the surface core of the PCUC flows at 150-200km from the coast with velocities more than 10 cm s^{-1} , in contrast with the equatoward PCC, which flows in the nearshore band (within 100 km from the coast) also with larger velocities of more than 15 cm s^{-1}. The increased vertical shear and the interaction (see section 2.5.5). with the topography favors the generation of mesoscale eddies, as seen in the high levels of eddy kinetic energy in the region. The role of these anticyclonic eddies become a key factor in recovering the normal conditions after the anomalously water intrusion. An injection of negative vorticity along the shelf during the intrusion phase, leads to a generation of positive vorticity in the nearshore band wich are release as mesoscale anticyclonic eddies with larger eddy lenght scales. These eddies might act counteracting the development of this ENSO feature, transportating in their cores non-anomalous water masses against the tongue far beyond the shelf. . Although the impact of eddies in Pisco are beyond the scope of our study, great progress have been done on tracking and describing their biological implicances. (Stramma et al., 2013). During LN phase, larger cross−shore velocities (8 cm s^{-1}) reveals that the major contribution of the enhanced upwelled waters belongs to depths between 50-100m, meanwhile the majority of the inorganic nutrients are still in the core of the deeper PCUC (300m) , so this could be a counter-productive fact that we are going to analyze with caution in future studies.

A coastally trapped PCUC is simulated in the three cases at San Juan (Figure 2.16). The subsurface equatoward current during EN conditions is the strongest, helping the NHCS to advect offshore, anomalous subsurface water masses, reducing productivity. Coastal upwelling, although weaker, still occurs. The cross-shore velocities exhibit a vertical shear, associated with the thermal-wind balance, showing high levels of eddy

activity, leading to strong horizontal density fronts in these region. During LN , the density gradient is southeastward (as wind-enhanced upwelling process brings denser waters begining from the south) and during EN, the density gradient switch direction, northwestward, leading to a verticall shear of the cross-shore velocity. In general San Juan and Pisco, present this relatively shallow upwelling with regards to the principal source of nutrients (PCUC).

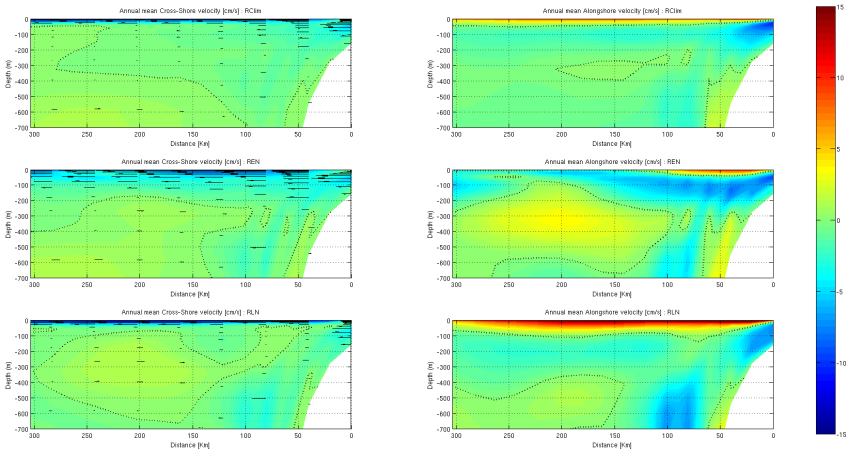

Figure 2.12: Vertical sections of annual mean cross-shore and alongshore velocities at Punta Falsa during climatological, El Niño and La Niña conditions.

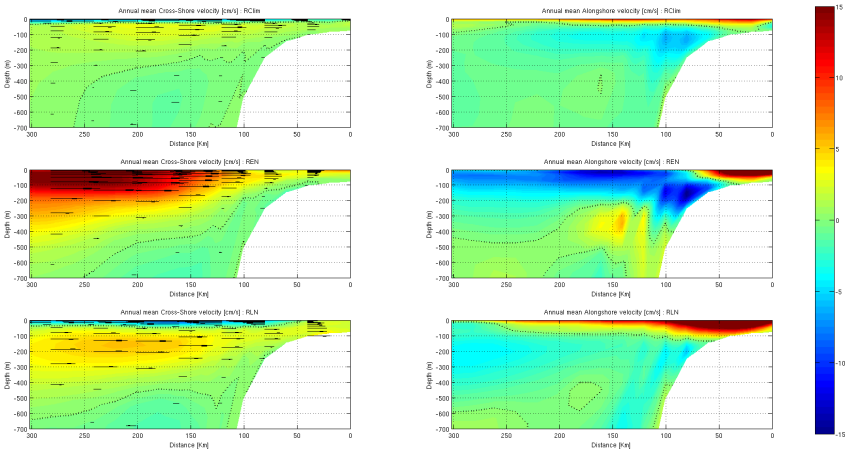

Figure 2.13: Vertical sections of annual mean cross-shore and alongshore velocities at Chimbote during climatological, El Niño and La Niña conditions.

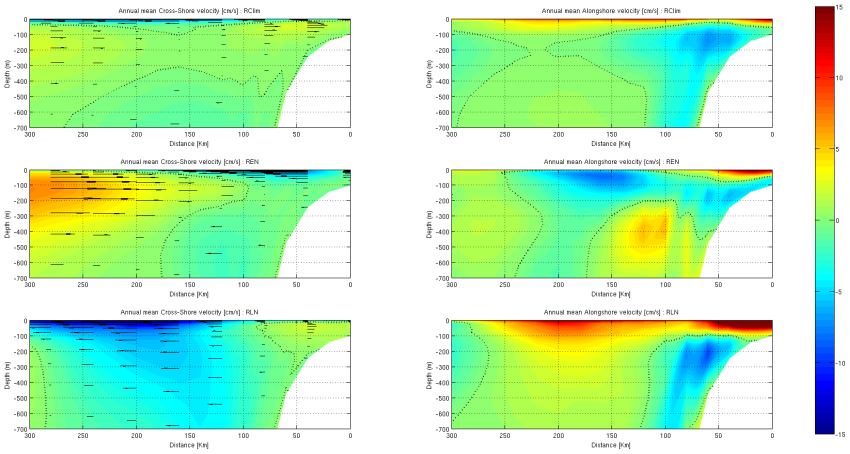

Figure 2.14: Vertical sections of annual mean cross-shore and alongshore velocities at Callao during climatological, El Niño and La Niña conditions.

2.5.2 ENSO signal

The Empirical Orthogonal Function (EOF) method is a map-series method of analysis that takes all the variability in the time−evolving field and breaks it into a few standing oscillations and a time series to go with each oscillation; each of these oscillations (each EOF) is often referred to as a mode of variability and their respective expansion coeffi-

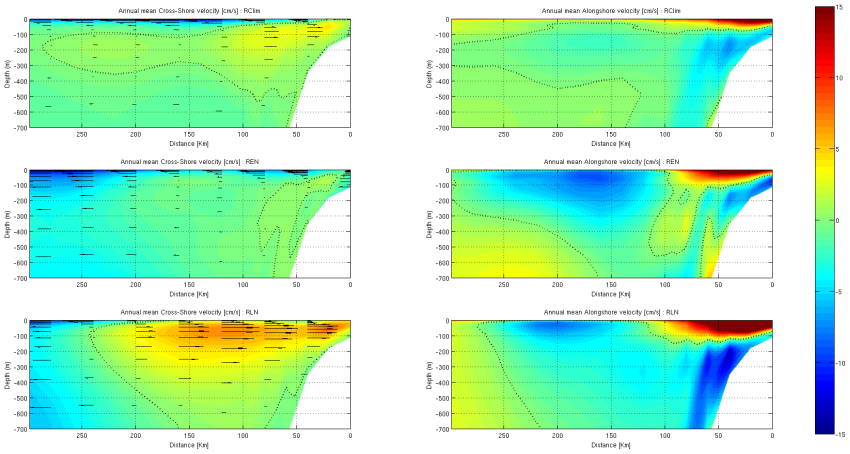

Figure 2.15: Vertical sections of annual mean cross-shore and alongshore velocities at Pisco during climatological, El Niño and La Niña conditions.

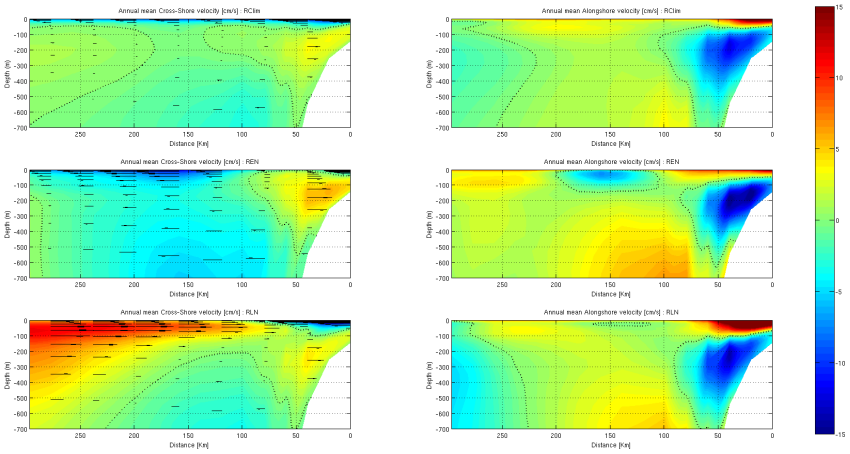

Figure 2.16: Vertical sections of annual mean cross-shore and alongshore velocities at San Juan during climatological, El Niño and La Niña conditions.

cients of the mode (Principal Component) show how this mode oscillates in time, so we performed an EOF analysis in order to find the spatial patterns of variability, their time variation, and obtain a measure of the importance of each pattern. To remove the annual cycle (predominant signal) of the surface fields (SST, NO_3, Chla) we applied the EOF analysis to their respective anomaly fields and now we are able to identify a slower

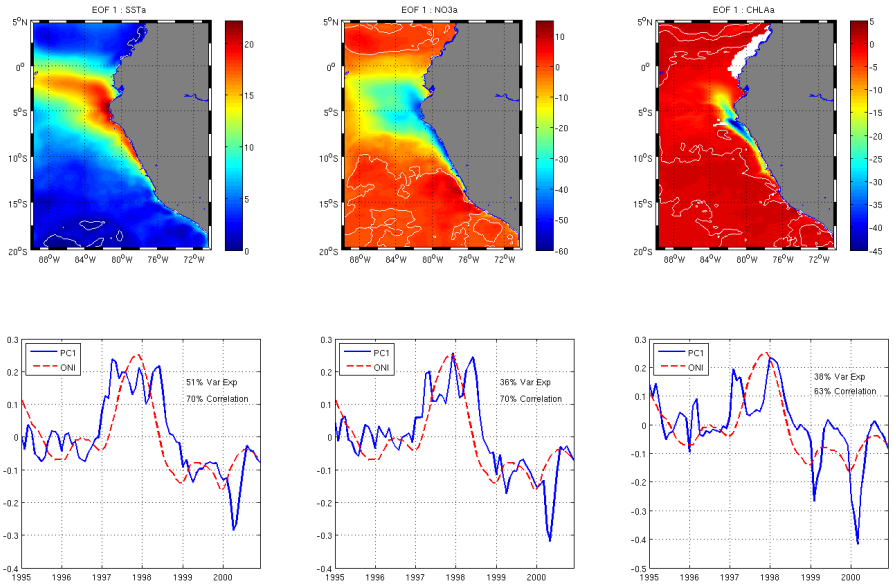

Figure 2.17: First mode of variability (EOF1) with their respective Principal Component(PC) for SST anomaly, NO_3 anomaly and Chlorophyll-a anomaly computed over the entire domain and over 1995-2000 period. White contour line are zero values. Oceanic Niño Index (10^1) is also plotted with each PC, positive values indicates EL phase and negative, LN.

major mode of variability and assume that everything else found in the observations is just noise.

The first mode of variability EOF1 of SST anomaly represents 51% of the total variance and their respective principal component PC1 is highly correlated 70% respect with the Oceanic Niño Index (10^{+1} ONI). These finding implies that the highly affected domain, showed as red colors in EFO1:SSTa (see Figure 2.17), reaches the highest anomaly values of $\pm 5°C$ at EN and LN respectively in agreement with mean historical values. For surface nitrate, the EOF1 explained just 36% of the variance but it is also highly ONI correlated (about 70%). Similarly as nitrate, the chlorophyll anomaly spatial pattern presents a coastal band (blue colors) where the variability

becomes extremely intense along these 6 year period of analysis; one can notice a strong fluctuation at chlorophyll concentrations; low levels of chla (negative anomaly about -8 mg m^{-3}) during EL phase, and high levels of chla (positive anomaly more than +10 mg m^{-3}) during LN, so ENSO events are leading the chlorophyll-a concentrations, distribution of nutrients and primary production as well.

Although all of principal components appears to be out of phase, we attribute these lag (about 3 months: cross correlation not shown) to the ONI seasonal values computed as a 3-month mean, and also because our experiment was not performed as a restricted interannual simulation and we keep the 30 days climatological month duration. A periodicity of about 4.5 years was detected in our signal of variability performed with the EOF, which is highly related with the periodicity of ENSO's signal (periodogram not shown). The results show a highly affected region extending offshore from Pisco following a non-veering coastline northwestward related with the anomalously equatorial water masses entering southeastward during EL and with the intensification of cold upwelled water along the coast, spreading it offshore by a strong horizontal advection. (see section 2.5.5)

2.5.3 Biogeochemistry

Oxygen Minimum Zone

The NHCS goes across a ventilation phase (Figure 2.18) during EN (as opossite during LN) due to an intrusion of equatorial surface and subsurface waters that oxygenates the water column lead, carrying oxygen-rich waters from the equatorial band. Eastward flows called primary and secondary Southern Subsurface Countercurrents: pSSCC and sSSCC, also known as Tsuchiya jets, were identified in Montes et al. (2014) as important contributors in oxygen content balance that enter the domain, with the sSSCC bringing low oxygen concentrations, and the pSSCC, elevated ones (nevertheless not as high as EUC associated waters).

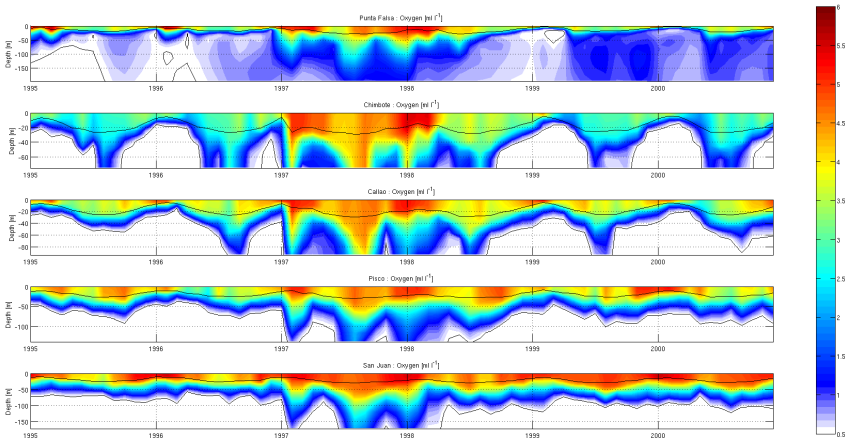

Figure 2.18: Time-depth diagram of oxygen concentrations [ml O_2 l^{-1}] during 1995-2000 simulated period. Upper black line represents the mixer layer and the deeper and irregular black contour, the top edge of the OMZ.

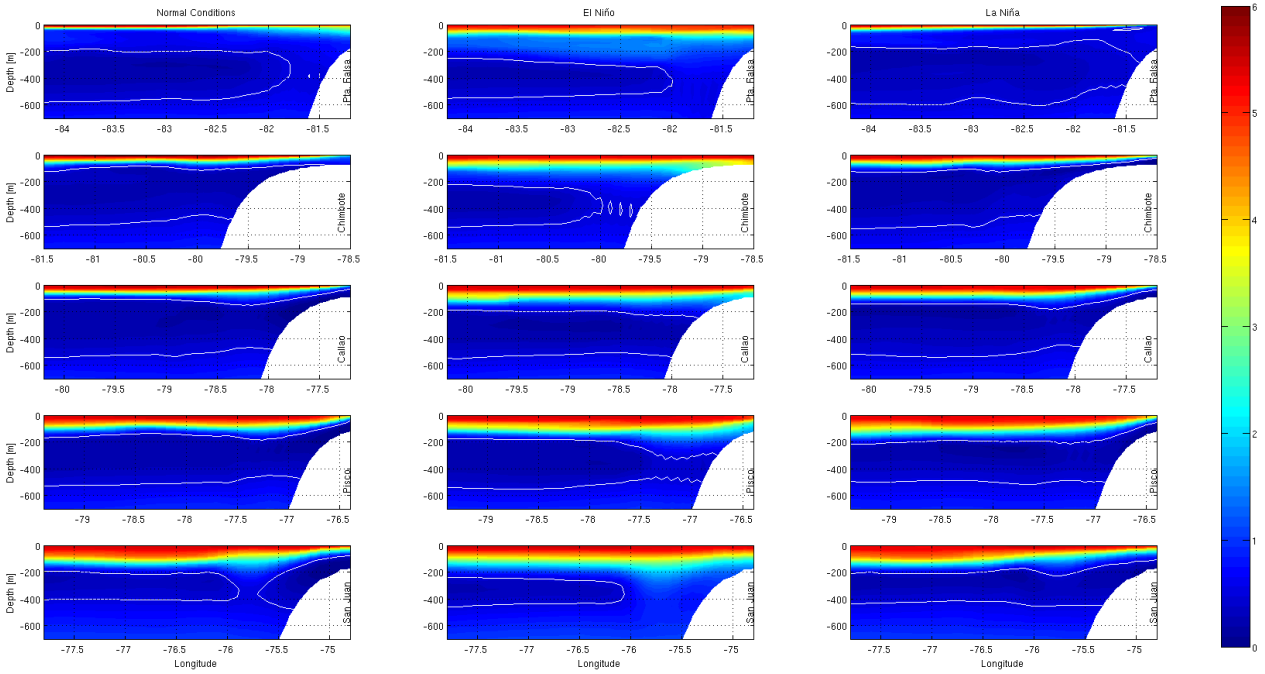

Figure 2.19: Vertical sections of oxygen concentration [mL L^{-1}] at Punta Falsa, Chimbote, Callao, Pisco and San Juan. Normal, EN and LN conditions are related to Rclim, 1997 and 1999 respectively. White contour represents the edges of OMZ (25 mmol O_2 m^{-3} or 0.5 mL O_2 L^{-1}). All sections were plotted at about the distance of 330 Km from the coast

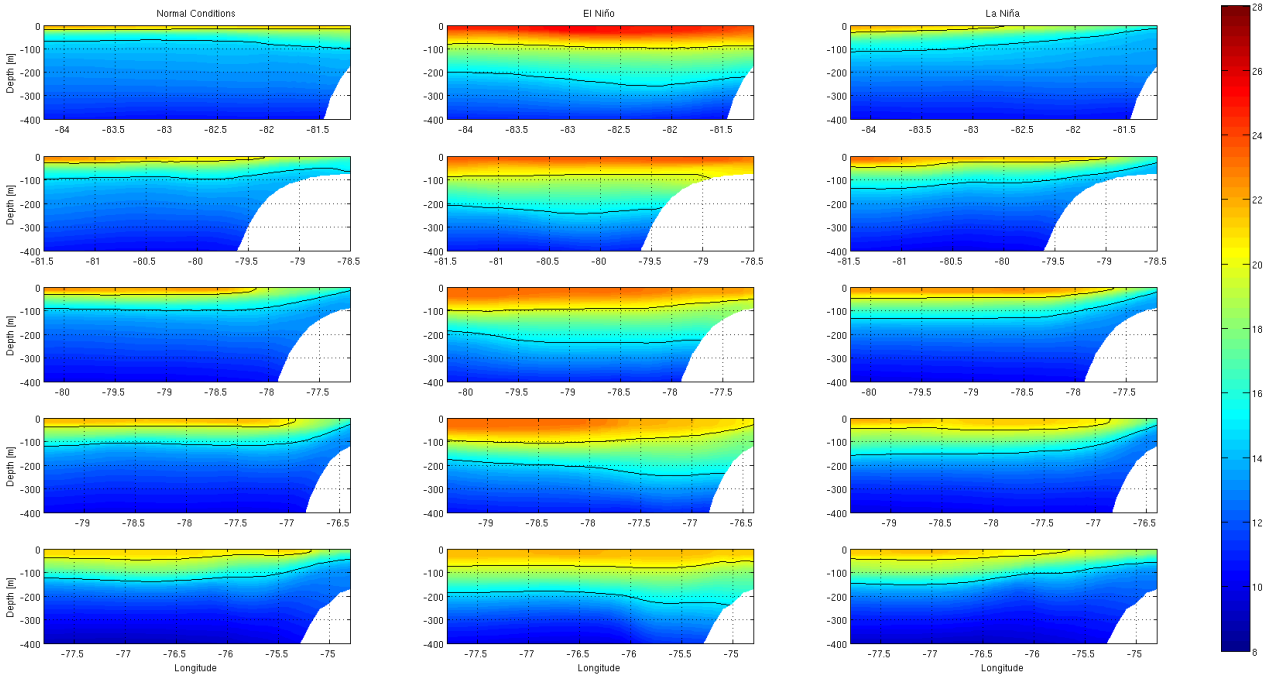

Figure 2.20: Vertical sections of temperature [°C] at Punta Falsa, Chimbote, Callao, Pisco and San Juan. Normal, EN and LN conditions are related to RClim, 1997 and 1999 respectively . Black contours represents the isotherms of 15 °C and 20 °C. All sections were plotted at about the distance of 330 Km from the coast

As expected, figure 2.19 shows that the top edge of the OMZ (white contour line of 0.5 mL L^{-1}) experiences a deepening and a strong offshore displacement during EN phase at all locations in agreement with the vertical structure of dissolved oxygen concentrations from in situ observations in Gutiérrez et al. (2008). Punta Falsa (the northernmost location) is very sensitive to ENSO variability due to its proximity to the Equator. One can note that the OMZ intercepts the shelf break during LN event, and it is located more than 80 km offshore at about 400 m depth during EN. A stratified, low density and warm upper layer of water, is developed which ventilates the coastal area, deepening the thermocline (see Figure 2.20, 2.21) and also the nutricline. This is because the variability of nutrients exhibits a similar temporal pattern related with the temperature due to their seasonal correlation following the intensity of the upwelling events along the year (Calienes et al., 1985).

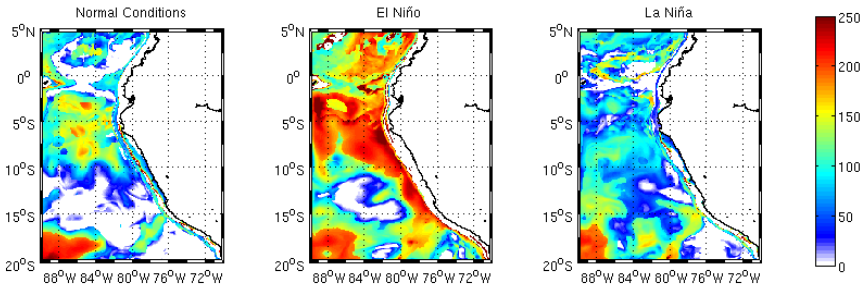

Figure 2.21: Depth [m] of isotherm of 15°C during Normal, EN and LN conditions.

At Chimbote, the difference between EN and LN are also very large, with important consequences for the local biogeochemistry. The continental shelf presents high levels of oxygen concentrations during EN while during LN, the OMZ spans all over the continental shelf, outcropping onshore due to enhenced upwelling and high biological activity related with a wide shelf, intense vertical mixing and non PAR limitation. Callao and Pisco are quite similar to Chimbote, presenting a very shallow OMZ, which deepens during EN events, oxygenating the first 150 m at shelf break. Pisco presents

a weakening OMZ whereas is getting closer to the coast. This narrow shape induces a thicker ventilated surface water mass (in relation with northern locations) that brings physical anomalies to the coast. San Juan displays a very different oxygen vertical distribution too. During EN, strong stratification of the upper ocean is established with a retracted OMZ tongue offshore, about 155 Km from the coast and 300 m depth when comparing with LN or non ENSO conditions in which it reaches the shelf at about 50-100 m depth in agreement with Minas et al. (1990).

In general, our results show the OMZ in the NHCS, at the coast, is shallower shoreward and southward in agreement with Codispoti and Packard (1980). In Chile, a deepening of the top edge of the OMZ and their retraction has been also observed, increasing the oxygen concentration in the upper 100m (Morales et al., 1999). In all locations, the deepening of the 15 °C isotherm (from shallower depths to more than 200m in our simulations) is sucessfully reproduced (Gutiérrez et al., 2005). On the other hand, LN has an opossite effect, outcropping the OMZ and deoxygenating the water column at the coast. (Wooster and Gilmartin (1961),Graco et al. (2007)).

Denitrification and Anammox

Nitrogen is one of the most biologically important element and also the most common limiting resource in the ocean and understanding the relationships between the different forms of nitrogen which belongs to a very complex biogeochemical cycle, is needed. The microbial activity in charge of the cycling of nitrogen through different ecosystem compartments might be quantified by modelling implicitely these processes within suboxic regions in the ocean that enhances the removal from it by anaerobic microbes which reduce nitrogen species for energy. Nitrate is the preferred electron acceptor because it is thermodynamically more effective after O_2, and it is consuming is referred as the respiration of nitrate in the absence of oxygen. For decades, it was assumed that was

from heterotrophic denitrification (a stepwise reduction process involving a number of intermediates $NO_3 \rightarrow NO_2 \rightarrow NO \rightarrow N_2O \uparrow \rightarrow N_2 \uparrow$) releasing the unwanted N_2O gas as an intermediate product, however the recently discovery of the anaerobic ammonium oxidation by nitrite (Anammox), as another pathway of lossing of N_2 in also suboxic conditions, occurs together with the well known denitrification process, except that anammox bacteria uses nitrite and ammonium in the environment to generate energy, skipping the generation of N_2O gas, but also contributing on the removal of fixed nitrogen in the ocean to the atmosphere.

We roughly assessed the relative contributions of the nitrogen lost by denitrification and anammox for each five locations during different physical conditions (EN,LN). We calculate the denitrification rate as a sum of the contribution of small detritus, large detritus and dissolved organic nitrogen (DON) for both stages of denitrification; the anammox rate were computed as described in Gutknecht et al. (2013a) using the formulation of Yakushev et al. (2007). All quantities were depth−integrated. (see Figure 2.22).

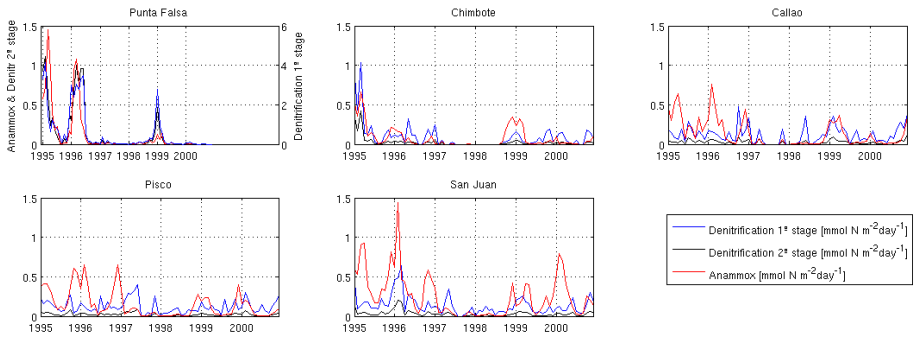

Figure 2.22: Rate of suboxic processes [mmol N $m^{-2}day^{-1}$], anammox against denitrification, both vertically integrated.

During normal conditions, anammox is imposed on denitrification only at the two southern locations, Pisco and San Juan, contributing to about 71% of nitrogen removal, with also an important 29% at Callao. In Chimbote and Punta Falsa this process does not seem very important . During EN conditions, anammox activity is strongly reduced but small fluctuations in the oxygen content allow heterotrophic bacteria to take advantage of anammox, with suboxic activity mostly due to denitrification even at low rates. During LN conditions, Chimbote has the most extreme shift, from 5% in neutral ENSO conditions thru almost 53% in LN conditions. Callao with 50%, Pisco with 47% and San Juan with 33%, meanwhile Punta Falsa remains with low contribution of anammox (5% on average) against denitrification. Babbin et al. (2014) suggest that, on average, 70% of the nitrogen lost in the ocean is a result of denitrification and 30% is lost through anammox (using N/C ratio of 0.15), but depending on the type of food available over the time (wide range of N/C ratio), denitrification and anammox can have different relative contributions to total nitrogen loss.

As described in the last section, a ventilation phase during EN leads to a supression of these suboxic processes. Denitrification (first and second stage) activity takes place at the top edge of the OMZ in our simulations, decreasing in intensity southward where anammox appears to gain importance (see Figure 2.23), These two processes appear to balance each other. They are the two main pathways of nitrogen removal and are highly modulated by the environmental physical conditions in the NHCS.

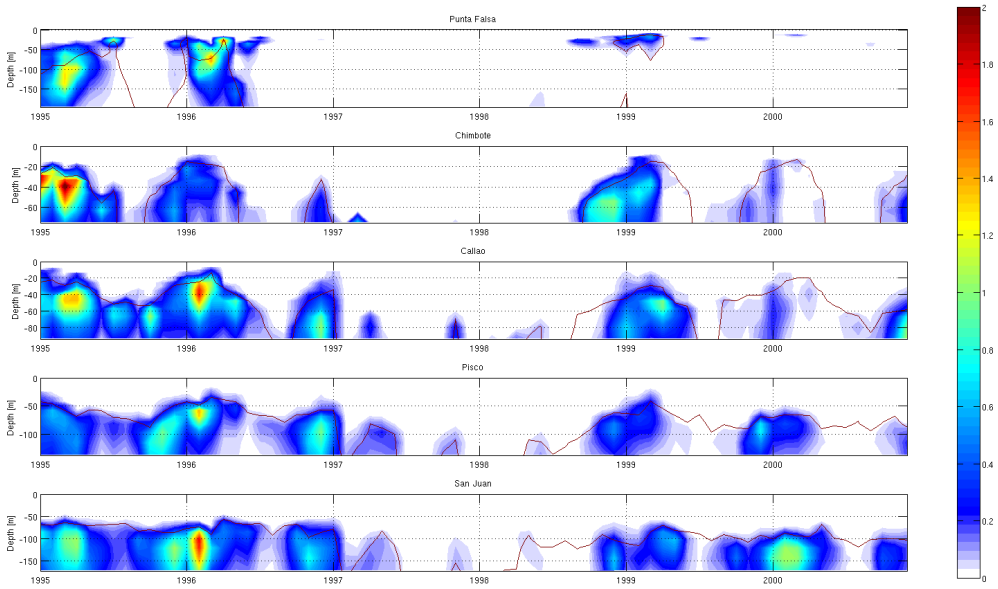

Figure 2.23: Anammox rate [mmol N $m^{-3}day^{-1}$]. Red contour represents the OMZ depth.

Nitrate

In this section we discuss the changes in temporal and vertical patterns of nitrate during ENSO events. Figure 2.24 shows a time-depth diagram for each of the 5 locations. Coastal upwelling and ENSO, important processes in the modulation of the spatiotemporal distribution of resources are well reproduced. The upwelling strength is associated with the SE trade winds that are commonly weak in summer and more intense in austral winter (Southern Hemisphere), so quite regular annual cycle is seen in the nitrate distribution during the 2 first years of simulation.

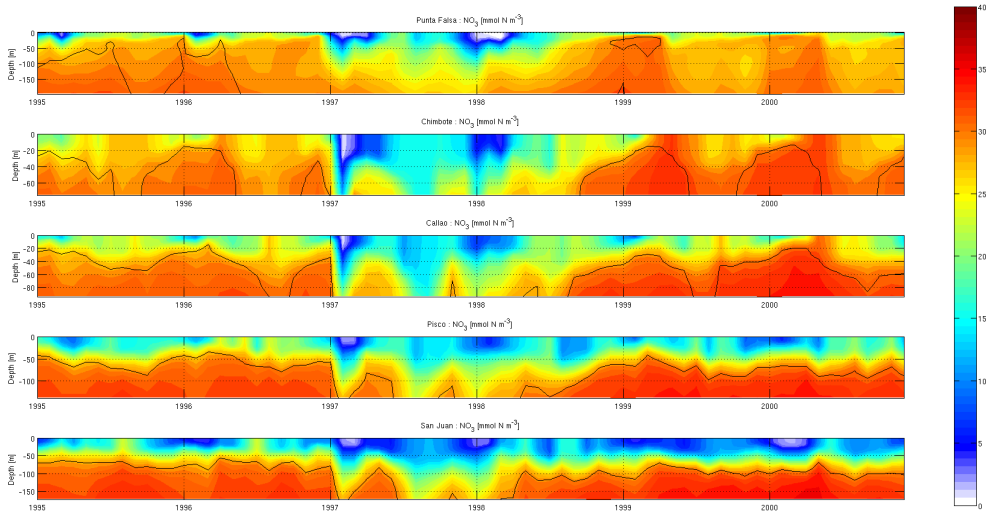

Figure 2.24: Time-depth diagram of nitrate concentration [mmol N m^{-3}] during 1995-2000 simulated period. Black contour line represents the top edge of the OMZ.

Very low concentrations of nitrate are reproduced with two strong peaks well defined in february-97 and january-98. The beginning of EN in the model results was seen along the Peruvian coast in March 97, earlier than in the observations. However, this lag will not affect our analysis because we will study the response of the biogeochemistry to physics from monthly−averaged model output. Maps of SST in the Climate Diagnostics Bulletin (NOAA 1997, 1998) report the development of a warm coastal tongue along the Peruvian border from february to april 1997 with a great equatorial transgression in february-97. A new instrusion ocurred during january-march 1998; therefore, despite a small lag, our results agree very well with observations. (see Figure 2.25).

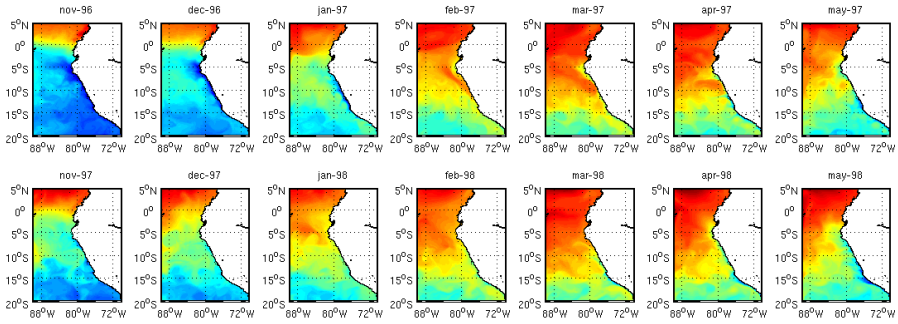

Figure 2.25: Sea surface temperature [°C] outputs. Note the two equatorial transgressions, first peak from february to april 1997, the second peak from january to march 1998.

During these two peaks, extremely low nitrate concentrations (less than 1 mmol N m^{-3}) were measured south of Callao and a remarkable feature also reproduced is related with concentrations < 5 mmol N m^{-3} of nitrate, which were also found above 100 m depth along almost all the peruvian coast (Sanchez et al., 2000).

During La Niña transition, extreme minimum values of nitrates are found in the upper layer at the southernmost locations, contradicting what normally is expected. Punta Falsa, Chimbote and also Callao, experience strong upwelling events, which replenish the upper layer with nutrients, enhancing primary productivity. The lack of nitrates found at Pisco and especially at San Juan, might be partially explained by the enhanced mesoscale eddy activity which would help advect coastal nutrients offshore into the oligotrophic ocean Gruber et al. (2011). In order to examinate this possibility, we look at the budget of nitrate concentrations, from the advective-diffusive equation in section 2.2. The physical (horizontal and vertical advection and diffusion) and biogeochemical (assimilation by phytoplankton and first stage of denitrification as sinks terms, and the second stage of nitrification, as a source term) contributions, where hadv (mixing) is the sum of zonal and meridional advection (difussion), vadv is the vertical advection term, and SMS is related to the sum of all the biological

process described previously; all of the mentioned quantities were vertically integrated for displaying as a time series at the 5 locations (see Figure 2.26).

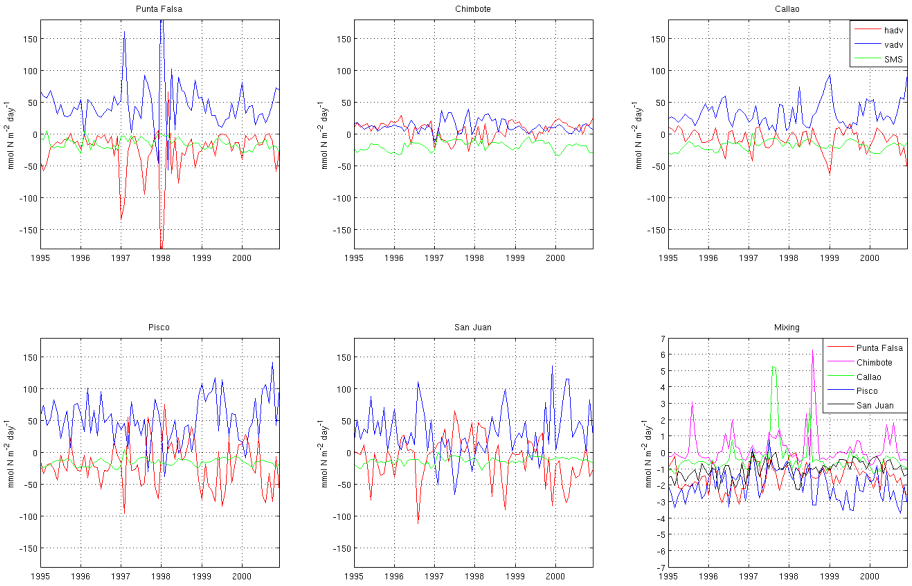

Figure 2.26: Budget of nitrate: Time series of flux of nitrogen due to physical (horizontal and vertical advection and diffusion) and biogeochemical (assimilation by phytoplankton and first stage of denitrification as sinks terms, and the second stage of nitrification, as a source term) contribution, where hadv (mixing) is the sum of zonal and meridional advection (difussion), vadv is the vertical advection term, and SMS is related to the sum of all the biological process described previously; all of the mentioned quantities were vertically integrated. Mixing processes were displayed separetaly for scaling.

Positive values indicates a favorable contribution (input or generation of N) and negative values indicates unfavorable contribution (leaking or consumption of N). In general nitrate appears to be controlled mostly by the horizontal and vertical advection with a minor contribution from the biology (SMS amplitudes), while mixing terms are an order smaller than the other processes. Punta Falsa, Pisco and San Juan exhibits a common bias during ENSO events, a crossing of signal that is greater at San Juan, which reveals a counterproductive contribution of vertical flux of nitrogen (nutrient poor waters), meanwhile a positive mean horizontal advection promotes the retention and

accumulation of particles (as inorganic nutrients even though at lower concentrations) at the coast by on-shore geostrophic flows which can limit the offshore dispersion and maintains anomalously warm water adjacent to the peruvian shelf during El Niño; these mechanism was demonstrated in Colas et al. (2008) using a Lagrangian experiment.

The biological contributions (SMS) gain relative importance when the physical terms are weaker, as Chimbote and also Callao, but in general the biology consumes nitrate at a small rate during El Niño (between 1-6 times less than La Niña, being 6 times at Punta Falsa and decaying southward); these latitudinal differences remain unexplained but could be associated with the level of ventilation related to the different water masses that spans our domain, with the equatorial subsurface currents bringing more oxygenated water masses during La Niña (Montes et al., 2011), thereby enhancing the nitrification processes.

Nitrite

The nitrites (NO_2^-) can be produced (bacterial activity) or excreted (by phytoplankton), and represent an intermediate oxidation state between ammonium and nitrate. Their presence reflects an unstable state in the system as it suggested by Graco et al. (2007). The source terms that BioEBUS takes into account are the first steps of nitrification (oxic process) and denitrification (suboxic process), meanwhile the sink terms are phytoplankton uptaking, anammox (suboxic process) and the second steps of nitrification (oxic process) and denitrification (suboxic process). We are emphasize the oxygen−dependent processes because the OMZ might play an important role in the distribution of nitrite. High levels of nitrite concentrations are detected at surface and subsurface levels , Codispoti et al. (1985). Two peaks along the water column known as Primary Nitrite Maximum (PNM) and Secondary Nitrite Maximum (SNM) are succesfully simulated as we can see at figure 2.27; but with greater discrepances in the right amplitudes of their concentrations. in situ measurements report that the PMN in the northern domain ranges between $0.1 - 3.5$ μM, at southern domain, SNM range between $1.0 - 5.5$ μM. After EN 1972, the nearshore coastal band raised nitrite concentrations more than 7.0 μM , Codispoti et al. (1985) and also after EN 1982-83, more than 1.0 μM were found. During LN 1974-75, the SNM were found at 100m depth with 11 μM. Dugdale et al. (1977).

The shallower peak of nitrites (PNM), is developed within the first 50 m deep in the nearshore region, at 50 km off the coast where oxygen concentrations are higher than the deventilated upwelled waters at the coast. This maximum arise under oxic conditions and it is accumulation is due the enhancing first step of nitrification (ammonium oxidation to nitrite in presence of oxygen) and also due to extracelular liberation of nitrite during the assimiliation of nitrate by the phytoplankton (exudation). On the other hand, the SNM is located between $100 - 250$ m deep and on the shelf, except

for northernmost location (6 °S) in agreement with (Codispoti and Packard, 1980), Fiadeiro et al. (1968). arguing that the northern limit of the SNM could be explained by the control exerted by the oxygenated inflow associated with the EUC.

The SNM increases due to an enhanced first step of denitrification (nitrate reduction to nitrite in absence of oxygen), therefore, when comparing with figure 2.19 (see also the white line in figure 2.27 for the top OMZ edge), the core of the SNM appears to occupy the upper OMZ in all cases. As expected, during EN, the oxygenation phase leads to a deepening, retirement, desintensification and in some cases, as Punta Falsa, a disappearance of the SNM, which, during normal conditions the coastal inventory of nitrite were initially supplied by these two oxic and suboxic processes. During EN phase our 5 locations still have nitrite at the coast, however they do not exhibit a decay of nitrite at the very nearshore region due to an increment of ammonium (see Figure 2.28), enhancing nitrification and counterbalancing the lack of the suboxic supplying nitrite mechanism (first step of denitrification).

During LN phase, another biological adjustment takes place, due the more oxygen−poor waters at the coast, the shallower oxic mechanism is constrained and the pool of nitrite might be maintained with the only suboxic mechanism which is now enhanced, following the core of the OMZ that intercepts the continental shelf as it is noticiable in all locations. Summarizing, both processes (first stages of nitrification and denitrification) are simultaneous and balance each other in terms of nitrite content during ENSO events. This vertical discontinuity (gap between maximum nitrites) becomes thicker during EN and thinner during LN phase leading to high levels of nitrite at shallower depths, indicating an additional supply of nitrite, which clearly comes from the upper OMZ, signifying a cool ENSO phase. A weakening or even a disappearance of the SNM, indicates a warm El Niño phase.

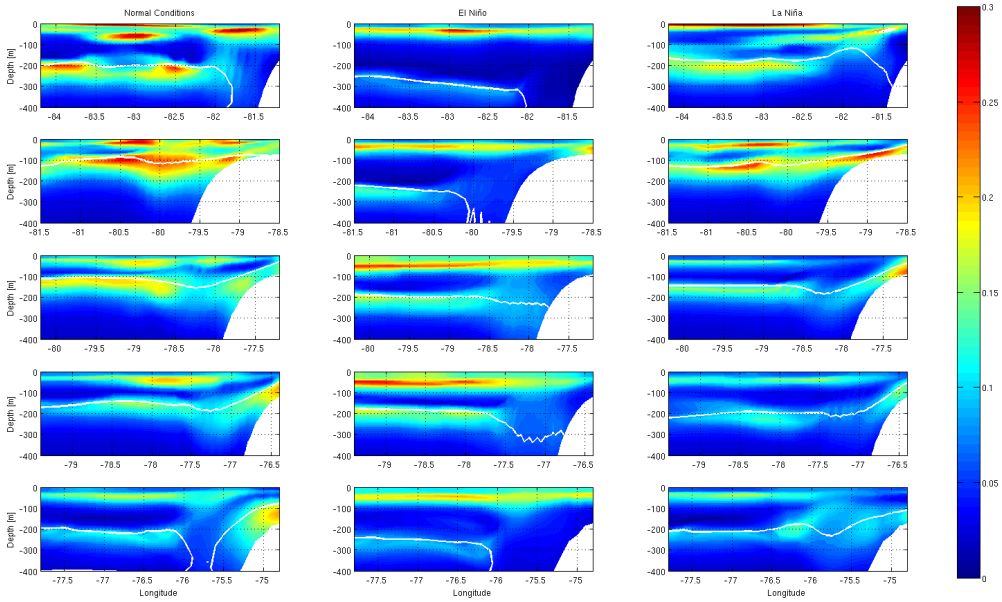

Figure 2.27: Vertical sections of nitrite [mmol N m^{-3}]. White line indicates the top edge of OMZ.

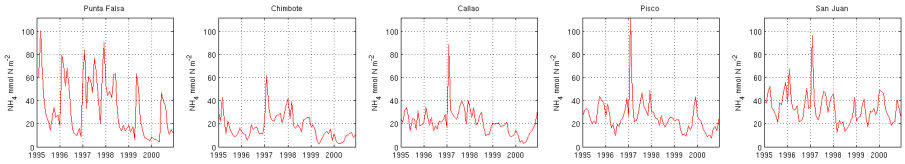

Figure 2.28: Time series of ammonium concentrations vertically integrated [mmol N m^{-}]

2.5.4 Primary production

The Primary Production were vertically integrated for each type of phytoplankton (large and small) in order to assess the temporal and latitudinal variability during ENSO events. Figure 2.29 shows a time series, where the blue line is for small phytoplankton (flagellates) and red line for large phytoplankton (diatoms), representing the main phytoplanktonic communitites in the NHCS.

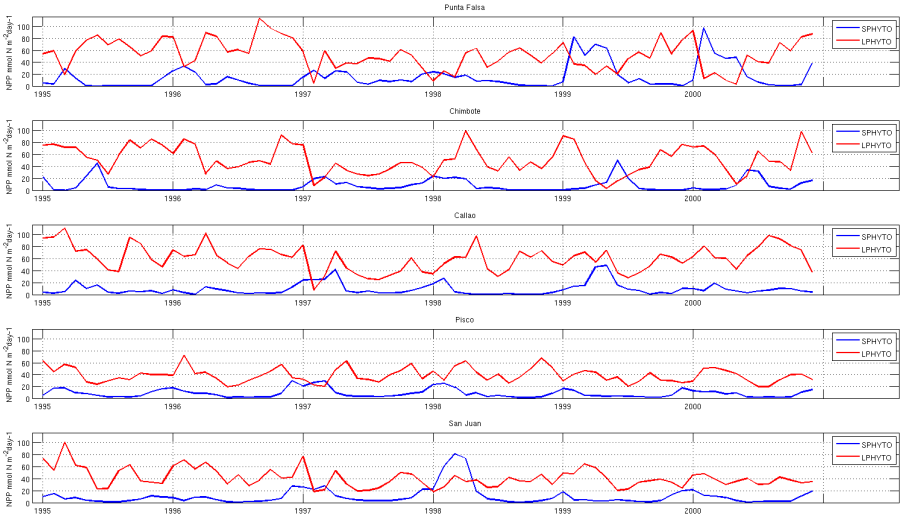

Figure 2.29: Primary production vertically integrated, in [mmol N m^{-2} day $^{-1}$] for each location during ENSO events. Blue line is for small phytoplankton (flagellates) and red line for large phytoplankton (diatoms).

Results show a decay of the PP during EN phase and an increase during LN phase; As we go further south, a weaker correlation between PP and ENSO signal is observed. Punta Falsa exhibits the largest changes, the most abrupt decay in the begining of 1997 and an increase in growth after EN peaks. Two well defined peaks of PP occur due to small phytoplankton during LN phase, while large phytoplankton go through a reduction phase. SPHYTO activity appears to be enhanced in the face of a drop in LPHYTO activity. From San Juan to Punta Falsa, one can notice a retardation of LN peaks as

we go northward, just observing the SPHYTO peaks between 1999-2000. SPHYTO is also very susceptible to the warm ENSO phase, peaking during the onset EN-1997 and early EN-1998, favored over LPHYTO, due a poor nutrient environment and their adaptability to low nutrient concentrations within smaller requirements than larger cells.

To understand the factors that controls these differences in the levels of primary production, we calculate the limitations terms for phytoplankton growth, a physical term related with the light avaliability for photosynthesis (PAR) and temperature; and a chemical term related with the inorganic nutrients limitation (nitrate, nitrite and ammonium). These two factors were vertically integrated and normalized (for qualitatively comparison between the quantities) and their difference were plotted as a time series (see Figure 2.30). Positive values (between 0 and 1) imply limitation by the chemical term (lack of nutrients) and negative values (between -1 and 0) imply limitation by the physical term (light−temperature).

During EN phase (1997-98), as expected, the lack of nutrients is the main controlling factor on primary production in all locations and the principal difference between large and small phytoplankton is the amplitude of the physical limitation term (negative peak in the middle 1997) explaining the major activity of large phytoplankton over the small one, where SPHYTO appears to be more affected by the physical changes between the two peaks of this warm phase. On the other hand, during LN phase (1999-2000), as well as during neutral conditions, the primary production becomes limited by the physics, due to the cold upwelled waters, which limit the growth rate of phytoplankton, as Eppley formulation described.

San Juan exhibits a different patterns during this cool phase, as seen in early 1999 and 2000 (peaks LN), the nutrient limitation term becomes important when compar-

ing with the physical conditions, revealing somehow a horizontal leaking of nutrients instead a lack of it, as occurs during EN phase; due to physical processes described in the section 6.5, supporting the mesoscale activity as an important modulating factor.

In summary, the PP under normal conditions follows a seasonal cycle, being non limited by the physics during spring-summer (warm and stratified waters) but becoming limited by nutrients as long as they are consumed. The rest of the year appears to be controlled by the physical changes in the environment. During EN phase, large phytoplankton activity is constrained, while small phytoplankton is locally enhanced, counter balancing each other. During LN phase, Punta Falsa, Chimbote, Callao and Pisco exhibits almost the same response (the level of correlation decrease as we go southward), however, at the southnermost location (San Juan), the interannual variability appears not to be the main factor in controlling the primary production and an additional hypotheses were tested in the next section in order to undestand the impact of the mesoscale activity, and their relation with the coastal inventory of nutrients in the two southern locations.

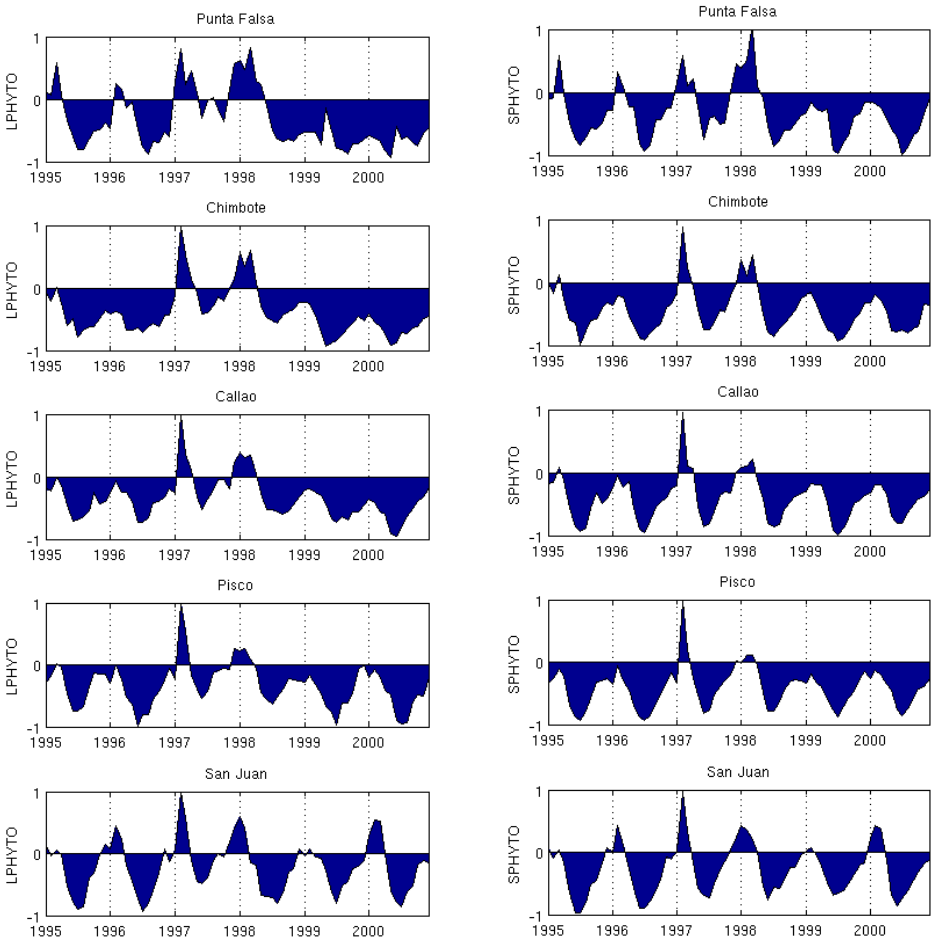

(a) Limitations factors for LPHYTO

(b) Limitations factors for SPHYTO

Figure 2.30: Difference between the two normalized growth rates limitation (physical and chemical term), both vertically integrated. Positive values is related with the importance of the lack of nutrients and negative values, with light or temperature limitation.

2.5.5 Impact of the wind and topography

Paracas peninsula is located just south of Pisco. Cape causes a maximum negative wind stress curl (see Figure 2.31) uplifting the Peru-Chile undercurrent (PCUC) (Albert et al., 2010), as Sverdrup theory predicts (also deepening southward due to the conservation of potential vorticity (Penven, 2005)).

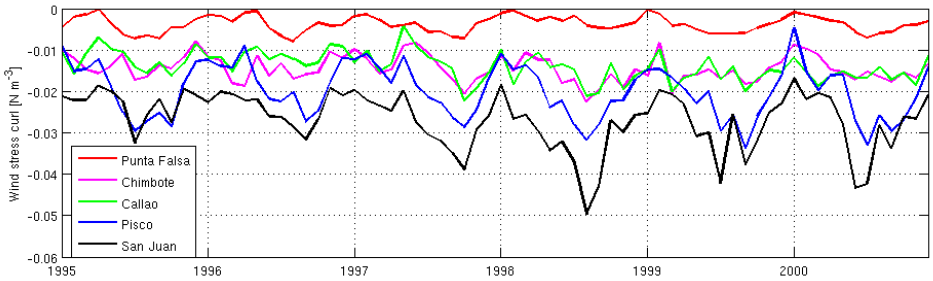

Figure 2.31: Wind stress curl N m^{-3}.

Maps of EKE reveals that the peninsula acts as a topography obstacle for wind stress (due to their nearness of the eastern part of the South Pacific subtropical anticyclonic gyre) and also for velocity fields (see figure 2.32) . This leads to an intense offshore Ekman transport (due to alongshore wind stress component) during LN phase and also during EN phase (in situ measurements demonstrate it). The weakening of the wind stress becomes noticiable at high latitudes and the apparent no reduction of winds fields during EN phase can be explained by onshore flows, in which the air right over the land is much warmer than the air right above the sea and as a result, the air pressure over the warm land is lower than the air pressure over the relative cool ocean, these different preassures causes wind, as the air moves from areas of higher pressure towards areas of lower pressure encounter a topography obstacle, the Andes mountain, veering equatoward flowing as a pseudo alongshore wind stress. Time series of offshore Ekman transport estimated from the alongshore wind stress component (Figure 2.33) shows an increase of the transport (more negative) during winter, associated with winter

time, the relaxation period of EN 1997, the recovery period of 1998 and LN periods of 1999-2000. Also there exists a relative increment of the transport during ENSO events at the two southern locations.

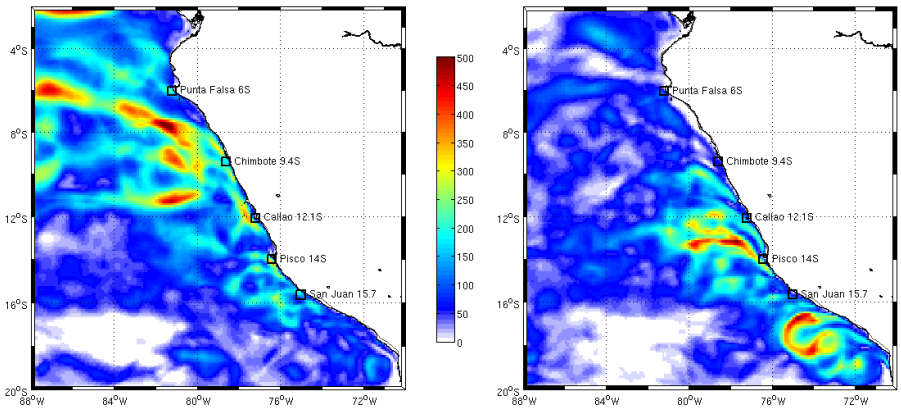

Figure 2.32: Annual mean Eddy Kinetic Energy cm^2s^{-2}. Left image is for year 1997 (El Niño) and right image, for year 1999 (La Niña).

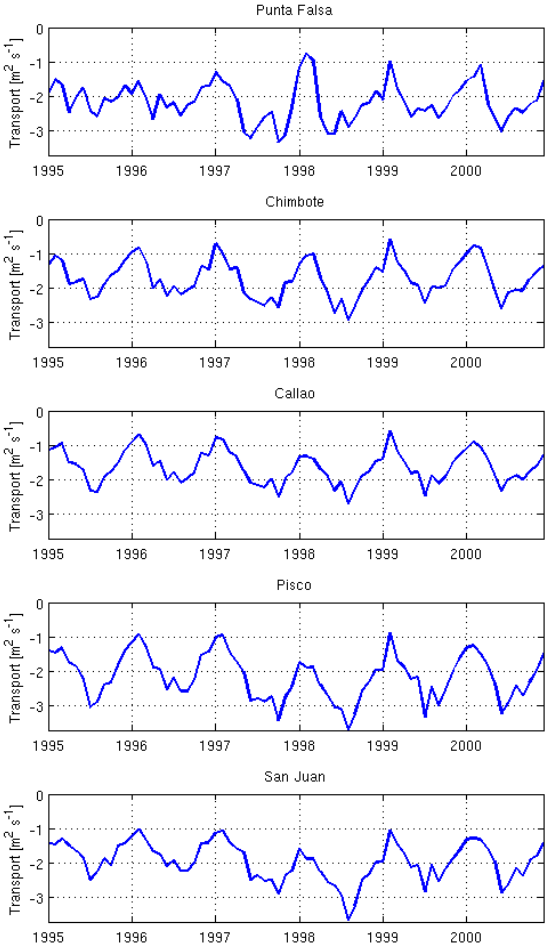

Figure 2.33: Ekman transport estimated from alongshore wind stress $m^2\ s^{-1}$.

The bend of the coastline at 14°S (Pisco) was proposed in Colas et al. (2008) as a critical factor in controlling the southward intrusion of equatorial anomalous water mass during El Niño; in order to test this hypotheses we create another experiment recreating the El Niño intrusion with the same lateral and surface boundary conditions used for the interannual simulations from 1995 to 2000, running only the physics (here-

after RnoPar). The coastline of the grid of RnoPar have been edited, cutting Paracas Peninsula as far as south of San Juan, keeping a regular constant coastline inclination (at about 53° related with horizon). In general, the surface and subsurface currents are still represented without relevant changes on the mean regional circulation (not shown), which allows us to proceed with the evaluation of the physical tracers for identification of these intrusive signal.

Figure 2.34 shows the surface monthly averaged Kinetic Energy (KE) in cm^2s^{-2} from january to march of 1997 for ilustrating the three stages of the process, january for the onset of the intrusion (february) , and march for the retraction of the anomalous water masses which were tracked following the density front using the isopycnal of 23.5 (black line) as a proxy. Velocity fields was also included (white arrows). The first row is related with the interannual simulation with no modifications at the coastline, and the second row is for RnoPar, although the real coastline was superimposed just for visualization.

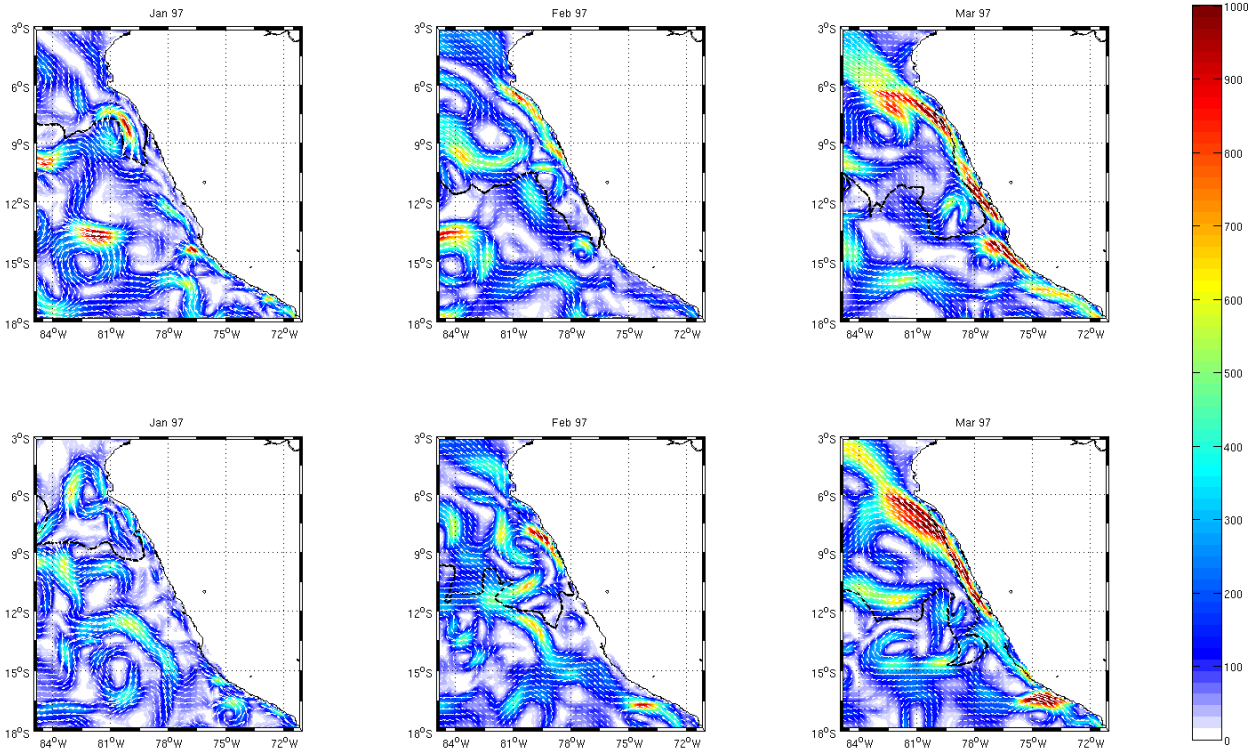

Figure 2.34: Kinetic Energy [cm^2s^{-2}] during the intrusion of the anomalous water masses (following the isopycnal of 23.6 as a proxy: black line) between january-march of 1997. The first row is for the interannual simulation (with no modifications at the coastline) and the second row, for RnoPar (simulation without Pisco-Paracas). White arrows are the velocity fields.

Cape Paracas presents high levels of energy because the convergence of the flow coming from southeast, that energy appears to be used as stronger offshore advections that Rnopar displays when veering as the oceanic branch of the PCC (between 78°W-81°W and 12°S-15°S). During the onset (january), a more energetic tongue is approaching southward around 9°S in the interannual simulation, that is not ocurring in Rnopar, due to a nearshore alongshore equatoward flow that Rnopar exhibits, that appears to be generated because the Peru Coastal Current (PCC) is now able to flow with no constrainment at a very nearshore region, weakening the intrusive southward tongue; this can be considered as a remote important consequence.

During the intrusion phase (february) the anomalous water masses reaches Pisco in agreement with figure 2.25 (section 4.4), while Rnopar exhibits a spatial retraction of 250 Km offshore south of Callao. Important quantity of momentum (fed from the south) is accumulated and then scattered in this region, so open it just release available energy in the system which has a supress effect against the anomalous water intrusion. In general, Pisco−Paracas acts as a shield against the PCC, meanwhile in RnoPar, it flows with no constrainment in the nearshore band pushing away the anomalous water masses 300 km northernmost. In march, RnoPar exhibits stronger alongshore equatoward fluxes than the interannual run. Rnopar also exhibits an irregular front which in the 3-day animation (not shown) is constantly modulated by the horizontal fluxes as we can see at 14°S-78°W directly associated with the coastal current, however in the real scenario, the Pisco-Paracas feature appears to help the dispersion of the southern limit of anomalous water more effectively than RnoPar. However in the coastal band the retraction is greater in RnoPar, which reaches Punta Falsa instead Chimbote. The Pisco-Paracas deflection has an important implication, acting as a physical barrier against the coastal equatoward jet, extending southernmost the limit of the warm anomalous tongue.

2.5.6 Gases

In this section we focus on the fluxes of gases at ocean−atmosphere interface that ROMS−BioEBUS simulates, the oxygen and the nitrous oxide. Under neutral conditions, oligotrophic ocean behaves as a source of oxygen, in other words, ocean releases oxygen to the atmosphere, meanwhile, upwelling centers in the nearshore region, due to upwelling of oxygen poor waters and also due microbial activity, acts as a sink of oxygen (i.e ocean takes oxygen from the atmosphere), figure 2.35 shows these espatial distribuitions.

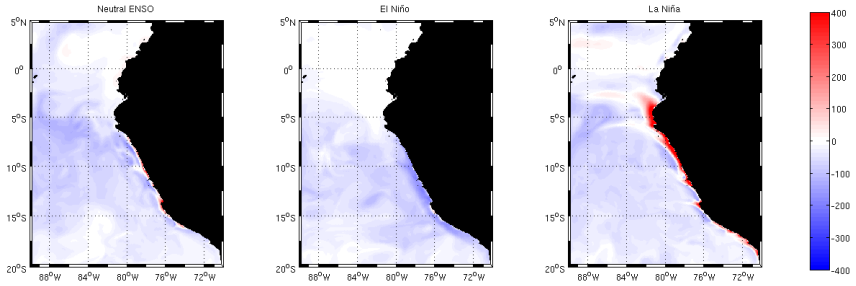

Figure 2.35: Flux of oxygen [mmol O_2 m^{-3} day^{-1}] at air-sea interface. Positive (negative) values indicate sink (source) of O_2.

As discussed in section 4.2, a ventilation phase ocurrs during EN leading nearshore region stops uptaking oxygen from atmosphere, furthermore, becomes a leaking region of oxygen, emmitting it at a mean rate of about 100 mmol O_2 m^{-3} day^{-1} or 2ml $l^{-1}day^{-1}$. On the other hand, LN brings more deoxygenated waters from the subsurface, and when they are in contact with the repleated atmosphere, promotes a vertical flux from the atmosphere to the ocean at high uptaking rates of more than 400 mmol O_2 m^{-3} day^{-1} or 11 ml $l^{-1}day^{-1}$ (at least 5 times stronger than El Niño emitting rate). We also bear in mind that biological activity acts producing oxygen, microbial activity consumes it,

and a delicated balance at the sea-air exchanges are leaded mostly by physical processes.

The picture for nitrous oxide (which in general their production increases exponentially with decreasing oxygen) is also expected (see Figure 2.36); no negatives values are shown because the model does not consume N_2O during the second step of denitrification which it occurs only at very low oxygen concentrations (Gruber, 2004) (Zamora et al., 2012), in spite of these caveat, we might proceed with the analysis.

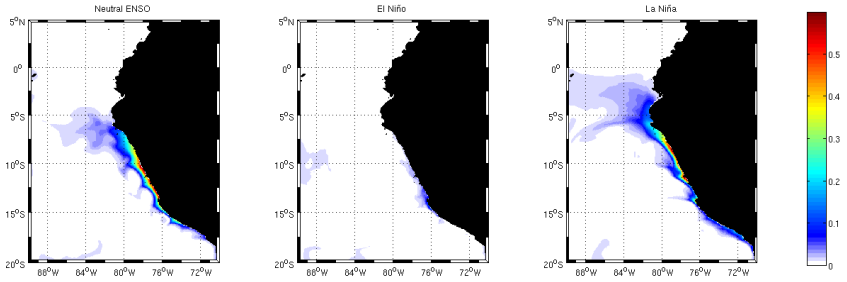

Figure 2.36: Flux of nitrous oxide [mmol N_2O m^{-3} day^{-1}] at air-sea interface. High values indicate source of N_2O.

Figure 2.37 shows a more detailed time series for nitrous oxide and also for oxygen at our 5 locations of study and their evolution during ENSO events, where high positive values of N_2O indicate an emmitting flux, and for O_2, indicate an uptaking flux.

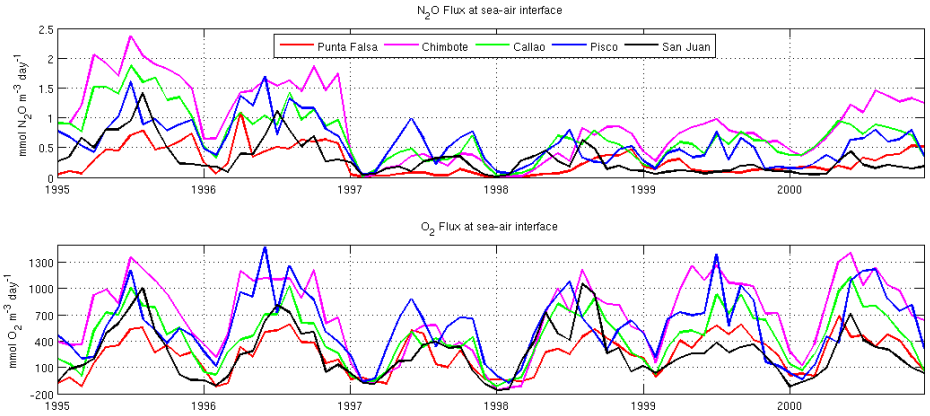

Figure 2.37: Flux of gases [mmol gas m^{-3} day^{-1}] at air-sea interface. Positive values for N_2O indicate a source flux and for O_2, a sink flux.

Chimbote appears to be a key location for gas exchange, emmitting N_2O at higher rates than other locations along the time series, except during EN phase, and can be partly explained due their width continental shelf, hosting more oxygenated warm water than the other ones, also the most drastic changes in terms of O_2 concentrations and the position of the OMZ occurs at Chimbote during EN phase, (see Figure 2.19) weakening their N_2O production. Comparing the proximity of the OMZ to the coast during LN phase with the emissions of N_2O to the atmosphere at each location, the following subject becomes clearly, the position and intense of the OMZ is directly related with releasing N_2O, in agreement with Suntharalingam et al. (2012), who suggest that an increase of N_2O production in the OMZ, should result in a similiar increase in N_2O outgassing, which explained the latitudinal difference in outgassing rate. A budget of N_2O was also performed (not shown) displaying almost the same temporal bias as nitrate budget presented at figure 2.26, revealing also the importance of advection as Gutknecht et al. (2013a) concluded, so we might propose use the outgassing N_2O as a proxy of the nearness of OMZ at the peruvian coast and also as a indicator of health of NHCS, because EN is clearly an mechanism that constrains this greenhouse effect gas emission; therefore, N_2O still deserves a further study.

2.6 Conclusions

We implemented a coupled physical-biogeochemical model ROMS-BioEBUS in order to assess how the physics controls biogeochemistry during ENSO events in the Northern Humboldt Current System. The 1995-2000 period was choosen for having two extreme ENSO events, El Niño 1997-1998 and La Niña 1999-2000; a detailed validation was performed using satellite derived data for the interannual simulations, databases and also in situ data for the climatological simulation. We were not focused in the weak El Niño of 1995 and the subsequent La Niña 1996 for our analysis due to some dynamical adjustments when starting simulating 1995, although the initial biogeochemical-physical state belongs to a statistically stable condition as described in section 4.2.3. Related with physical aspects, the coastal circulation, dominated by PCC and the PCUC, displays great alterations and latitudinal differences. During El Niño, the PCUC exhibits a horizontal spreading (250Km), an increase of the velocity (about 50% faster), a slight uplifting at the slope but a sharply outcropping core between 100-150 km of the coast acting as a countercurrent. The equatoward coastal jet displays a nearshore band constrainment (first 100 km), becoming deeper (100m) and somewhat faster. Another important feature during EN phase is the appearance of the equatoward deep undercurrent with more than 5 cm s^{-1} at about 300-650 m deep and 50-180 km away from the coast. During LN phase, the PCUC remains faster and shallower than climatological conditions, but does not outcrops to the surface, except in Pisco and lesser at San Juan, meanwhile the PCC exhibits a general intensification within a thicker surface layer.

We reproduced a highly ENSO−affected region from the equatorial band to 16°S (San Juan) with a southeastward propagation. This southern limit is a result between physical interactions with Paracas Peninsula, which acts as a shield against the PCC, allowing anomalous water masses reach 300 km southernmost than if the bend of

the coastline of Pisco-Paracas never existed. We called this feature as the confluence between anomalous warm El Niño waters against cold Humboldt waters during the intrusion ENSO phase.

Due to Pisco-Paracas special physical characteristics, the leaking of coastal nutrients inventory becomes evident in our results. Low nitrate concentrations (< 5 mmol N m^{-3}) during LN events, with the strongest nitrate horizontal offshore advection in addition with stronger vertical advection of nitrate-poor waters that occurs at a very shallow depths (50m) while the nutricline is located deeper (below 100m). This lead a depletion of nutrients at the southern coastal region. We also have to take into consideration that the OMZ becomes shallower southward, leading to a reduction of the nitrification rates and enhacing of denitrification at the coast.

The OMZ experiences a sinking (on average 180m deeper than neutral phase) and a strong offshore displacement (on average 75km offshore than neutral phase) during EN phase due to the intrusion of equatorial surface and subsurface ventilated waters. The nearshore part of the OMZ in the NHCS, is shallower shoreward and southward under neutral conditions, meanwhile during LN phase, the OMZ spans over the continental shelf deventilating the nearshore coastal band. Chimbote exhibits larger changes during ENSO events, due to the nearness of equatorial variability and due their wider continental shelf (in relation with the other locations of study), hosting high levels of oxygen concentrations during EN and in contrast, during LN, an outcropping of the top edge of the OMZ at the coast due to high rates of biological activity and enhanced upwelling process, leads depleted oxygen waters.

Within the OMZ, important suboxic processes occurs, as anammox and denitrification; during neutral conditions, anammox is imposed on denitrification at Pisco and San Juan, contributing with about 71% (each one) of nitrogen removal, with also

an important 29% at Callao, meanwhile at Chimbote and Punta Falsa, denitrification is dominating the removal. During EN phase, anammox experiences a supression, in contrast during LN phase, where Chimbote reachs 53%, Callao 50%, Pisco 47% and San Juan 33% of the percentual contribution of nitrogen removal against denitrification; implying that the cool ENSO phase enhaced anammox rates from Chimbote to San Juan, decreasing southward.

Two other microbial activities that control the pool of nitrite concentrations at the surface and subsurface were reproduced; the first step of nitrification (under oxic conditions) leads the Primary Nitrite Maximum (PNM) in the first 50m deep in the nearshore region, at 50 km from the coast, and the first step of denitrification (undex suboxic conditions), leading the Secondary Nitrite Maximum (SNM) at 100-250 m deep and onto the shelf, except for the northernmost location Punta Falsa, that could be modulated by the control exerted by the oxygenated inflow associated with the EUC. Results showed that the PNM is located somewhat above the top of the OMZ, whereas the SNM is located in the upper layer of the OMZ, so El Niño (ventilation phase) leads to a deepening, retraction, weakening and even a disappearance (as at Punta Falsa) of the SNM. During LN (deventilated phase) constrains the PNM (now located offshore and shallower) and enhances SNM at the coast. These oxygen dependent processes involved in the supplying mechanism of nitrite, could be used as an ENSO indicator, where the vertical discontinuity (gap between maximus of nitrite) becomes thicker during EN and thinner during LN, and the SMN clearly behaves as a proxy of the nearness of the OMZ core to the coast, and their disappearance is related with a warm El Niño phase.

Related with the primary production (PP), ENSO signal is the main modulating factor; EN phase leads a decay on PP, about 50% reduction for large phytoplankton in

contrast with a locally enhanced small phytoplankton activity, peaking meanwhile large phytoplankton does not get used to extremely low nutrient concentrations, counter balancing each other; however, small phytoplankton appears to be more affected by physical limitations than bigger cells.

On the other hand, during LN phase, PP becomes limited by the physics (cool upwelled waters) instead chemistry (vertical supplying of nutrients); however, San Juan is the only location which displays also nutrient limitation, confirming our suspicions about the leaking of nutrients in southern locations due to mesoscale activity as Gruber et al. (2011) described, furthermore, the level of correlation between ENSO signal and its influence on PP (positive or negative) gets weaker as we go southward. Large cells appears to be more susceptible than small ones.

Finally, we also quantified the gas interchange fluxes at the sea−air interface and we concluded that EN phase leads to a constrainment of the greenhouse N_2O gas emission, which during LN phase becomes an intensified source with a horizontal expansion of the emmitting area, spanning over the equatorial band. The O_2 gas is emmited at a mean rate of about 100 mmol O_2 m^{-3} day^{-1} during EN, meanwhile is uptaked at a mean rate of about 400 mmol O_2 m^{-3} day^{-1} during LN at the coastal band. We also propose use the outgassing N_2O as a proxy of the nearness of OMZ at the peruvian coast and also as an indicator of health of NHCS, where strong decay of emissions might be related with the warm phase of El Niño.

Chapter 3

Final Considerations

We could assess the main changes of physical and biogeochemical processes in the NHCS during ENSO events, and as we have shown in this work, El Niño leads to an important reduction on primary production but somehow it also deserves to be seen as a redemptive phase, in which one of the main important elements on earth (oxygen) is now provided, in which one of the main important greenhouse gas (nitrous oxide) is now constrained and stop emitted to our polluted atmosphere and where the ocean heat content (given by the sun) is now released, consuming this energy by evaporation and also relieving the temperature distribuition on earth; we can not see ENSO as isolated oceanographic phenomenon, because as we known, it is a coupled atmospheric−oceanographical event that affects directly the Pacific Ocean, and more precisely, the coasts of Peru where great efforts are being made by Instituto del Mar del Peru, Dirección de Hidrografía y Navegación, Instituto Geofísico del Peru, Senamhi and Indeci, providing weakly and dayly bulletins for monitoring thermal conditions at peruvian coasts.

Propose new long term biogeochemical indicators and describe general responses for a better understanding of climatic variability and ENSO cycle, were suggested in

this work as important contributions.

In spite of not having yet a realistic representative physical−biogeochemical model for NHCS, due to their complexity, we believe that the results are important insights in how a climatological biogeochemistry will response with different physical scenarios, that results in a recreation of El Niño and also La Niña conditions; while it is true that we choosed specific ENSO years, we have to proceed with caution when quantifying biogeochemical rates, because the parameterization is already an approximation and different initial and boundary conditions leads to different results, however, the response and the bias of these interelated processes remains somehow invariant, and our findings may help to understand and predict how the NHCS will react during extreme events that are becoming frequently in the face of climatic changes.

Bibliography

Albert, a., Echevin, V., Lévy, M., and Aumont, O. (2010). Impact of nearshore wind stress curl on coastal circulation and primary productivity in the Peru upwelling system. *Journal of Geophysical Research*, 115(C12):C12033.

Babbin, A. R., Keil, R. G., Devol, A. H., and Ward, B. B. (2014). Organic matter stoichiometry, flux, and oxygen control nitrogen loss in the ocean. *science*, 344(6182):406–408.

Bange, H. W. (2006). Nitrous oxide and methane in European coastal waters. *Estuarine, Coastal and Shelf Science*, 70(3):361–374.

Behrenfeld, M. J. and Falkowski, P. G. (1997). Photosynthetic rates derived from satellite-based chlorophyll concentration. *Limnology and oceanography*, 42(1):1–20.

Belmadani, A., Echevin, V., Dewitte, B., and Colas, F. (2012). Equatorially forced intraseasonal propagations along the Peru-Chile coast and their relation with the nearshore eddy activity in 1992–2000: A modeling study. *Journal of Geophysical Research*, 117(C4):C04025.

Calienes, R., Guillén, O., and Lostaunau, N. (1985). Variabilidad espacio-tempral de clorofila, producción y nutrientes frente a la costa peruana.

Carr, M.-E. (2002). Evolution of 1996–1999 La Niña and El Niño conditions off the western coast of South America: A remote sensing perspective. *Journal of Geophysical Research*, 107(C12):3236.

Carton, J. a. and Giese, B. S. (2008). A Reanalysis of Ocean Climate Using Simple Ocean Data Assimilation (SODA). *Monthly Weather Review*, 136(8):2999–3017.

Casey, K. S., Brandon, T. B., Cornillon, P., and Evans, R. (2010). The past, present, and future of the avhrr pathfinder sst program. In *Oceanography from Space*, pages 273–287. Springer.

Codispoti, L. and Packard, T. (1980). Denitrification rates in the eastern tropical south-pacific. *Journal of marine research*, 38(3):453–477.

Colas, F., Capet, X., McWilliams, J., and Shchepetkin, a. (2008). 1997–1998 El Niño off Peru: A numerical study. *Progress in Oceanography*, 79(2-4):138–155.

Da Silva, A., Young, C., and Levitus, S. (1994). Atlas of surface marine data 1994, vol. 1, algorithms and procedures, noaa atlas nesdis 6. *US Department of Commerce, NOAA, NESDIS, USA*, page 74.

Echevin, V., Albert, A., Lévy, M., Graco, M., Aumont, O., Piétri, A., and Garric, G. (2014). Intraseasonal variability of nearshore productivity in the Northern Humboldt Current System: The role of coastal trapped waves. *Continental Shelf Research*, 73:14–30.

Echevin, V., Aumont, O., Ledesma, J., and Flores, G. (2008). The seasonal cycle of surface chlorophyll in the Peruvian upwelling system: A modelling study. *Progress in Oceanography*, 79(2-4):167–176.

Echevin, V., Colas, F., Chaigneau, A., and Penven, P. (2011). Sensitivity of the

Northern Humboldt Current System nearshore modeled circulation to initial and boundary conditions. *Journal of Geophysical Research*, 116(C7):C07002.

Fuenzalida, R., Schneider, W., Garcés-Vargas, J., Bravo, L., and Lange, C. (2009). Vertical and horizontal extension of the oxygen minimum zone in the eastern South Pacific Ocean. *Deep Sea Research Part II: Topical Studies in Oceanography*, 56(16):992–1003.

Graco, M. I., Ledesma, J., Flores, G., and Girón, M. (2007). Nutrientes, oxígeno y procesos biogeoquímicos en el sistema de surgencias de la corriente de humboldt frente a perú. *Revista peruana de biología*, 14(1):117–128.

Gruber, N. (2004). The dynamics of the marine nitrogen cycle and its influence on atmospheric co2 variations. In *The ocean carbon cycle and climate*, pages 97–148. Springer.

Gruber, N., Lachkar, Z., Frenzel, H., Marchesiello, P., Münnich, M., McWilliams, J. C., Nagai, T., and Plattner, G.-K. (2011). Eddy-induced reduction of biological production in eastern boundary upwelling systems. *Nature geoscience*, 4(11):787–792.

Gutiérrez, D., Aronés, K., Chang, F., Quipúzcoa, L., and Villanueva, P. (2005). Impacto de la variación oceanográfica estacional e inter-anual sobre los ensambles de microfitoplancton, mesozooplancton, ictioplancton y macrozoobentos de dos áreas costeras del norte del perú entre 1994 y 2002. *Bol. Inst. Mar Perú*, 22:3–60.

Gutiérrez, D., Enriquez, E., Purca, S., Quipúzcoa, L., Marquina, R., Flores, G., and Graco, M. (2008). Oxygenation episodes on the continental shelf of central peru: Remote forcing and benthic ecosystem response. *Progress in Oceanography*, 79(2):177–189.

Gutknecht, E., Dadou, I., Le Vu, B., Cambon, G., Sudre, J., Garçon, V., Machu, E., Rixen, T., Kock, a., Flohr, a., Paulmier, a., and Lavik, G. (2013a). Coupled physi-

cal/biogeochemical modeling including O₂-dependent processes in the Eastern Boundary Upwelling Systems: application in the Benguela. *Biogeosciences*, 10(6):3559–3591.

Gutknecht, E., Dadou, I., Marchesiello, P., Cambon, G., Le Vu, B., Sudre, J., Garçon, V., Machu, E., Rixen, T., Kock, a., Flohr, a., Paulmier, a., and Lavik, G. (2013b). Nitrogen transfers off Walvis Bay: a 3-D coupled physical/biogeochemical modeling approach in the Namibian upwelling system. *Biogeosciences*, 10(6):4117–4135.

Hooker, S. and McClain, C. (2000). The calibration and validation of seawifs data. *Progress in Oceanography*, 45(3):427–465.

Koné, V., Machu, E., Penven, P., Andersen, V., Garçon, V., Fréon, P., and Demarcq, H. (2005). Modeling the primary and secondary productions of the southern Benguela upwelling system: A comparative study through two biogeochemical models. *Global Biogeochemical Cycles*, 19(4):n/a–n/a.

Kosro, P. (2002). A poleward jet and an equatorward undercurrent observed off oregon and northern california, during the 1997–98 el nino. *Progress in Oceanography*, 54(1):343–360.

Lengaigne, M. (2002). Ocean response to the March 1997 Westerly Wind Event. *Journal of Geophysical Research*, 107(C12):8015.

Levitus, S., Antonov, J., Baranova, O., Boyer, T., Coleman, C., Garcia, H., Grodsky, A., Johnson, D., Locarnini, R., Mishonov, A., et al. (2013). The world ocean database. *Data Science Journal*, 12(0):WDS229–WDS234.

Liu, W. T., Tang, W., and Polito, P. S. (1998). Nasa scatterometer provides global ocean-surface wind fields with more structures than numerical weather prediction. *Geophysical Research Letters*, 25(6):761–764.

Marchesiello, P., McWilliams, J. C., and Shchepetkin, A. (2003). Equilibrium structure and dynamics of the california current system. *Journal of Physical Oceanography*, 33(4):753–783.

McClain, C. R. (1998). Science quality seawifs data fro global biosphere research. *Sea Technology*, 39:10–16.

Minas, H., Coste, B., Minas, M., and Raimbault, P. (1990). Conditions hydrologiques, chimiques et production primaire dans les upwellings du pérou et des iles galapagos, en régime dhiver austral (capagne paciprod). *Oceanologica Acta*, 10:383–391.

Montes, I., Colas, F., Capet, X., and Schneider, W. (2010). On the pathways of the equatorial subsurface currents in the eastern equatorial Pacific and their contributions to the Peru-Chile Undercurrent. *Journal of Geophysical Research*, 115(C9):C09003.

Montes, I., Dewitte, B., Gutknecht, E., Paulmier, A., Dadou, I., Oschlies, A., and Garçon, V. (2014). High-resolution modeling of the eastern tropical pacific oxygen minimum zone: Sensitivity to the tropical oceanic circulation. *Journal of Geophysical Research: Oceans*, 119(8):5515–5532.

Montes, I., Schneider, W., Colas, F., Blanke, B., and Echevin, V. (2011). Subsurface connections in the eastern tropical Pacific during La Niña 1999–2001 and El Niño 2002–2003. *Journal of Geophysical Research*, 116(C12):C12022.

Morales, C. E., Hormazábal, S. E., and Blanco, J. (1999). Interannual variability in the mesoscale distribution of the depth of the upper boundary of the oxygen minimum layer off northern chile (18–24s): Implications for the pelagic system and biogeochemical cycling. *Journal of Marine Research*, 57(6):909–932.

Morel, A., Berthon, J.-F., et al. (1989). Surface pigments, algal biomass profiles, and potential production of the euphotic layer: Relationships reinvestigated in view of remote-sensing applications. *Limnol. Oceanogr*, 34(8):1545–1562.

Nevison, C., Butler, J. H., and Elkins, J. W. (2003). Global distribution of N 2 O and the ΔN 2 O-AOU yield in the subsurface ocean. *Global Biogeochemical Cycles*, 17(4):n/a–n/a.

O'Reilly, J. E., Maritorena, S., Mitchell, B. G., Siegel, D. A., Carder, K. L., Garver, S. A., Kahru, M., and McClain, C. (1998). Ocean color chlorophyll algorithms for seawifs. *Journal of Geophysical Research: Oceans (1978–2012)*, 103(C11):24937–24953.

Paulmier, a. and Ruiz-Pino, D. (2009). Oxygen minimum zones (OMZs) in the modern ocean. *Progress in Oceanography*, 80(3-4):113–128.

Penven, P. (2005). Average circulation, seasonal cycle, and mesoscale dynamics of the Peru Current System: A modeling approach. *Journal of Geophysical Research*, 110(C10):C10021.

Penven, P., Marchesiello, P., Debreu, L., and Lefèvre, J. (2008). Software tools for pre- and post-processing of oceanic regional simulations. *Environmental Modelling & Software*, 23(5):660–662.

Pocklington, R. (1981). Organic matter in upwelling off northern perú, november 1977.

Saha, S., Moorthi, S., Pan, H.-L., Wu, X., Wang, J., Nadiga, S., Tripp, P., Kistler, R., Woollen, J., Behringer, D., Liu, H., Stokes, D., Grumbine, R., Gayno, G., Wang, J., Hou, Y.-T., Chuang, H.-Y., Juang, H.-M. H., Sela, J., Iredell, M., Treadon, R., Kleist, D., Van Delst, P., Keyser, D., Derber, J., Ek, M., Meng, J., Wei, H., Yang, R., Lord, S., Van Den Dool, H., Kumar, A., Wang, W., Long, C., Chelliah, M., Xue, Y., Huang, B., Schemm, J.-K., Ebisuzaki, W., Lin, R., Xie, P., Chen, M., Zhou, S., Higgins, W., Zou, C.-Z., Liu, Q., Chen, Y., Han, Y., Cucurull, L., Reynolds, R. W., Rutledge, G., and Goldberg, M. (2010). The NCEP Climate Forecast System Reanalysis. *Bulletin of the American Meteorological Society*, 91(8):1015–1057.

Sanchez, G., Calienes, R., and Zuta, S. (2000). The 1997-98 el niño and its effects on the coastal marine ecosystem off peru. *Reports of California Cooperative Oceanic Fisheries Investigations*, 41:62–86.

Shchepetkin, A. F. and McWilliams, J. C. (2005). The regional oceanic modeling system (ROMS): a split-explicit, free-surface, topography-following-coordinate oceanic model. *Ocean Modelling*, 9(4):347–404.

Shchepetkin, A. F. and McWilliams, J. C. (2009). Correction and commentary for "Ocean forecasting in terrain-following coordinates: Formulation and skill assessment of the regional ocean modeling system" by Haidvogel et al., J. Comp. Phys. 227, pp. 3595–3624. *Journal of Computational Physics*, 228(24):8985–9000.

Smith, W. H. and Sandwell, D. T. (1997). Global sea floor topography from satellite altimetry and ship depth soundings. *Science*, 277(5334):1956–1962.

Stramma, L., Bange, H. W., Czeschel, R., Lorenzo, A., and Frank, M. (2013). On the role of mesoscale eddies for the biological productivity and biogeochemistry in the eastern tropical pacific ocean off peru. *Biogeosciences (BG)*, 10(11):7293–7306.

Stramma, L., Johnson, G. C., Sprintall, J., and Mohrholz, V. (2008). Expanding oxygen-minimum zones in the tropical oceans. *science*, 320(5876):655–658.

Stramma, L., Schmidtko, S., Levin, L. a., and Johnson, G. C. (2010). Ocean oxygen minima expansions and their biological impacts. *Deep Sea Research Part I: Oceanographic Research Papers*, 57(4):587–595.

Strub, P. T., Mesías, J. M., Montecino, V., Rutlant, J., and Salinas, S. (1998). Strub et al 1998.pdf. In Robinson, A. R. and Brink, K. H., editors, *The Sea, Volume 11*, chapter Coastal oc, pages 273–314.

Suntharalingam, P., Buitenhuis, E., Le Quéré, C., Dentener, F., Nevison, C., Butler, J. H., Bange, H. W., and Forster, G. (2012). Quantifying the impact of anthropogenic nitrogen deposition on oceanic nitrous oxide. *Geophysical Research Letters*, 39(7).

Suntharalingam, P., Sarmiento, J., and Toggweiler, J. (2000). Global significance of nitrous-oxide production and transport from oceanic low-oxygen zones: A modeling study. *Global Biogeochemical Cycles*, 14(4):1353–1370.

Ulloa, O., Escribano, R., Hormazabal, S., Renato, A., Gonz, R. R., and Ramos, M. (2001). Evolution and biological effects of the 1997-98 El Ni ~ no in the upwelling ecosystem off northern Chile. 28(8):1591–1594.

Wooster, W. S. and Gilmartin, M. (1961). The peru-chile undercurrent. *Journal of Marine Research*, 19(3):97–122.

Yakushev, E., Pollehne, F., Jost, G., Kuznetsov, I., Schneider, B., and Umlauf, L. (2007). Analysis of the water column oxic/anoxic interface in the Black and Baltic seas with a numerical model. *Marine Chemistry*, 107(3):388–410.

Zamora, L., Oschlies, A., Bange, H. W., Craig, J., Huebert, K., Kock, A., and Löscher, C. (2012). Nitrous oxide dynamics in low oxygen regions of the pacific: insights from the memento database. *Biogeosciences (BG)*, 9:5007–5022.

Zuta, S. and Guillén, O. (1970). Oceanografía de las aguas costeras del perú.

Appendix A

SODAsim Vs ECCOsim

The two first experiments performed to choose a initial state and also to create a biological monthly climatology for the interannual run, were compared in order to avaliate the vertical estructure of the circulation in the NHCS. The following results were based following the validated outputs of 4 articles which modelated the surface and subsurface circulation in the NHCS: Penven (2005), Montes et al. (2010), Montes et al. (2011) and Echevin et al. (2011).

Figure A.1 shows the zonal currents [cm s^{-1}] that enter in our domain at the first 300 meters depth; red color are for positive velocities (shoreward) and blue ones, for negative velocities (offshore direction). In general, SODAsim exhibits a more defined subsurface (SSCCs and EUC) and surface (SEC) currents, also a stronger core of the EUC is well reproduced without the merging with the pSSCC displayed at ECCOsim. The values are in the range demostrated at the references showed at the begining, i.e , at the right latitude, depth and also intensity, being sSSCC between 6°S-7°S, the pSSCC between 3°S-4°S, , the EUC between 1.5°S-1.5°N and the SEC 2°S-2°N with 25-40 cm s^{-1}, and another southern branch at 5°S.

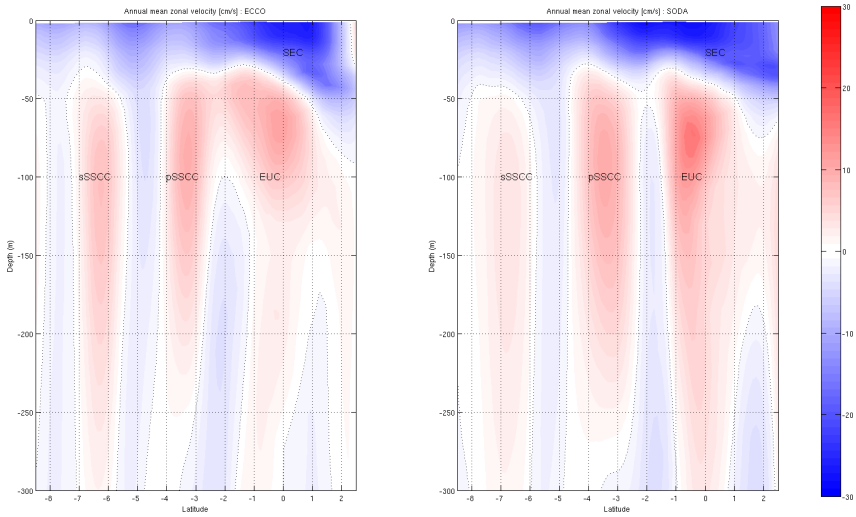

Figure A.1: Annual mean zonal velocities [cm s^{-1}] from ECCOsim and SODAsim averaged between 86°W and 87°W.

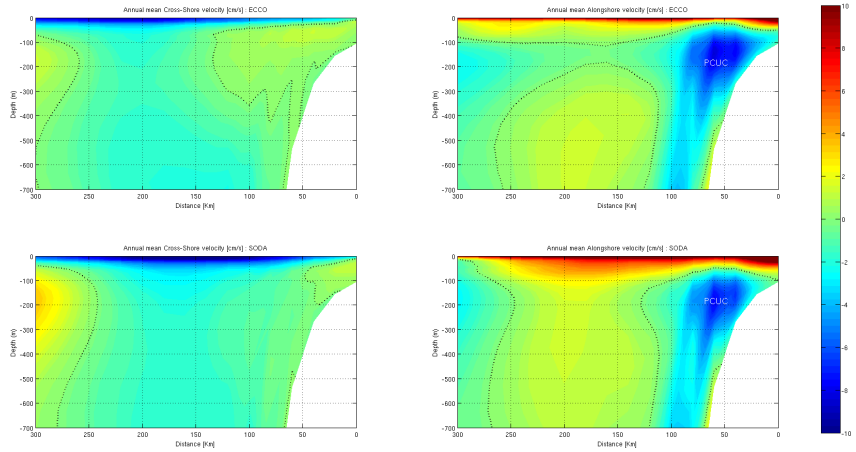

Figure A.2: Annual mean cross-shore (left) and alongshore (right) velocities [cm s^{-1}] from ECCOsim (first row) and SODAsim (second row) at Callao 12°S. Black dotted line are zero values.

Figure A.2 shows clearly the PCUC running poleward over the slope with a maximum core of 15 cm s^{-1} at a depth of 100-200 m, dominating the first 150 Km from the coast, extending about 700 m depth. again, ECCOsim exhibits an unreal wider

offshore extension (black dotted line) and a greater outcropping, trapping the coastal equatoward jet in a thinner layer at the coast than in SODAsim; furthermore a signature of the Peru-Chile Countercurrent (PCCC) appears at the western side of SODAsim shallower than ECCOsim, which is in agreement with literature.

Related with the cross-shore velocities, positive velocities indicate clearly onshore subsurface velocities related with upwelling processes, then advected offshore (blue negative velocities) in a thicker layer and more intense at SODAsim.

The facts exposed before leaded to choose the final physical state of SODAsim as initial conditions and also to using SODA as the OGCM which is going to force our interannual simulations.

Appendix B

Taylor Diagrams

Taylor diagrams is used to display graphically how closely a simulated variable (ROMS-BioEBUS output) matches with observations (database-satellite). In general, simulated patterns that agree well with observations will lie nearest the black dot ($x = 1; y = 0$); exhibiting a high correlation and low RMS error. Red arc is related with the centered pattern RMS error, so the distance between the simulated and observed pattern is proportional to the distance to the black dot (observation).

The figure B.1 shows Taylor diagram for sea surface temperature (A), sea surface salinity (B), oxygen (C) and also nitrate (D) for comparison between RClim outputs and climatological databases, as satellite derived data. Each color represent a season, blue for summer, red for fall, green for winter and yellow for spring; and the circle markers are comparisons against CARS2009 database and the cross markers, against MODIS (SST) or WOA2013 (SSS). It is also important to keep in mind that these analysis were performed for the entire domain.

Digram A shows that SST is highly correlated, (96% with CARS2009 and 95% with MODIS) and their variations are at the right amplitude ($\sigma = -0.5$ with CARS and $\sigma = +0.8$ with MODIS) leading to minor errors (inside the red rms arc).

Diagram B shows a good agreement in salinity field, very high correlations (97% with CARS2009 and 98% with WOA2013) and a minimum negative standard deviation close to the observation (black line radius). On the other hand, oxygen and nitrate fields are not as high correlated as temperature or salinity in relation with CARS2009; summer and fall are somehow not as well represented as winter and spring time. The simulation exhibits a more nutritive and less oxygenated surface in comparing with the climatological database. Note than in spite of surface oxygen concentrations displays about half correlation of temperature or salinity, still remain closer to the observated pattern (low standard deviation).

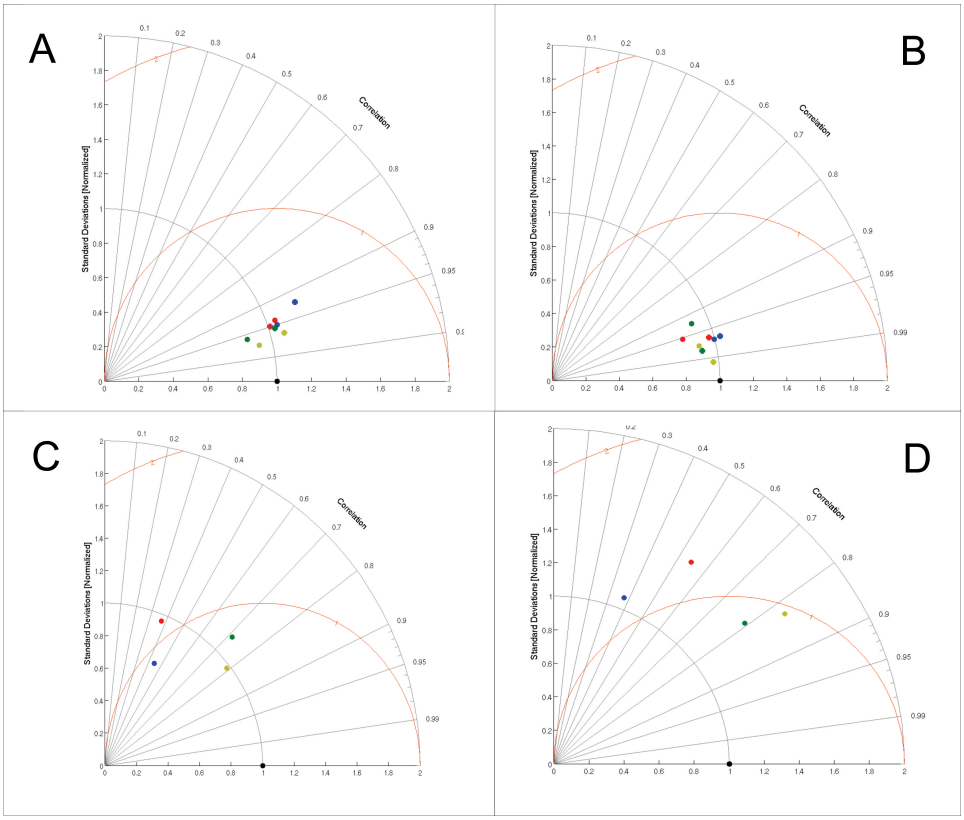

Figure B.1: Taylor diagram of model simulated A) sea surface temperature [°C] in comparison with CARS2009 (circles) and MODIS (cross); B) sea surface salinity in comparison with CARS2009 (circles) and WOA2013 (cross); C) Oxygen [mmol O_2 m^3] in comparison with CARS2009; D) Nitrate [mmol N m^3] in comparison with CARS2009. Blue markers are for summer, red for fall, green for winter and yellow for spring season. The black dot is for the observation (CARS2009, MODIS or WOA2013).

Appendix C

In situ data

In situ data were provided by Instituto del Mar del Perú (IMARPE) from several oceanographic cruises:

- Cruise 2003 (august)
- Cruise 2005 (march)
- Octavo Regional 2005 (october)
- Cruise Jurel 2008 (november-december)
- Pelágico 2012 (february-april)

They were all averaged for comparison against RClim (our climatological simulation) by constructing each month averaged over all available data for each specific region only where data were measured; only SST and SSS were performed (see Figure C.1 and C.2).

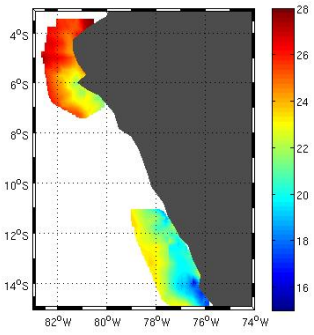

(a) SST [°C] IMARPE feb-apr 2012

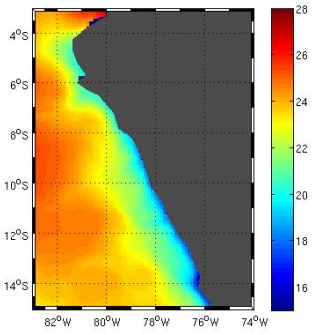

(b) ROMS [°C] averaged feb-apr

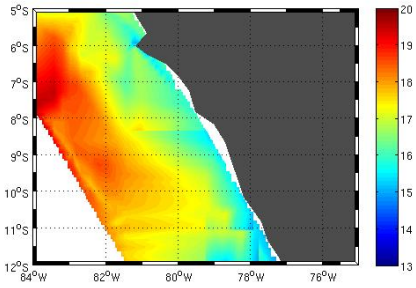

(c) SST [°C] IMARPE oct 2005

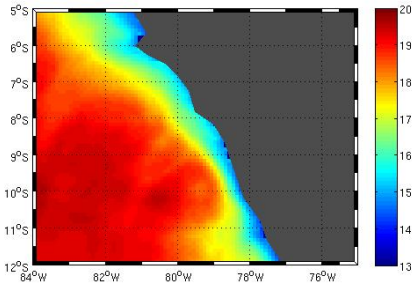

(d) ROMS [°C] averaged october

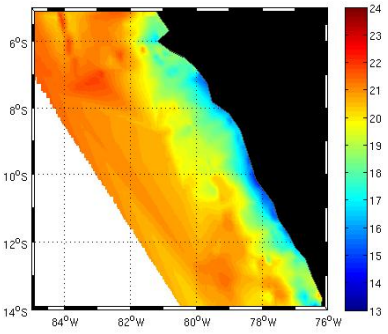

(e) SST [°C] IMARPE nov-dec 2008

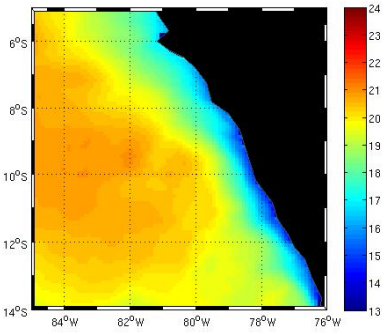

(f) ROMS [°C] averaged nov-dec

Figure C.1: Sea surface temperature [°C] comparison between IMARPE data and ROMS (RClim).

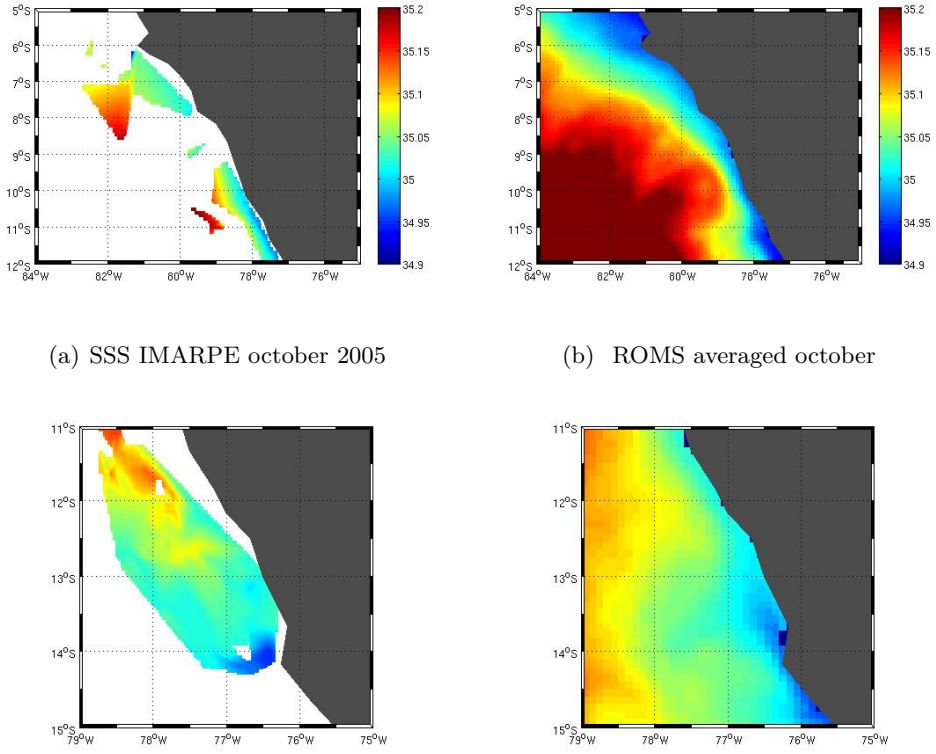

(a) SSS IMARPE october 2005

(b) ROMS averaged october

(c) SSS IMARPE august 2003

(d) ROMS averaged august

Figure C.2: Sea surface salinity comparison between IMARPE data and ROMS (RClim). Colorbar for bottom images are the same as the previous ones.

The temporal and spatial pattern are well represented in spite of been compared in situ data of specific years. ROMS is able to capture the most important features of the observed physical tracers due to the ability in resolving the mesoscale, and the discrepances, might be attributed to the use of a monthly mean forcings.